Cell Tissue Res (2017) 370:243–265
DOI 10.1007/s00441-017-2661-5

REGULAR ARTICLE

Morphology and ultrastructure of the tarsal adhesive organs of the Madagascar hissing cockroach *Gromphadorhina portentosa*

Christian Schmitt[1] · **Oliver Betz**[1]

Received: 24 November 2016 / Accepted: 15 June 2017 / Published online: 12 August 2017

Abstract The present transmission and scanning electron microscopic study of the ultramorphology of the pliable attachment pads (arolium, euplantulae) of the Madagascar hissing cockroach *Gromphadorhina portentosa* reveals structural evidence for their function in producing, storing, and secreting an adhesion-mediating secretion and releasing it to the exterior. The exocrine epidermal tissue of both the arolium and the euplantula is significantly enlarged by numerous invaginations stretching into the hemolymph cavity. Its cells show large nuclei, numerous mitochondria, Golgi complexes, and a prominent rough-surfaced endoplasmic reticulum integrated within an electron-dense cytoplasm that contains numerous vesicles of diverse electron density and size. Invaginations of the cell membrane provide evidence for strong membrane turnover. The glandular epithelium of both the arolium and the euplantula releases the adhesion-mediating secretion into a subcuticular void from which it has to permeate the thick cuticle of the adhesive pads. The subcuticular void is compartmentalized by cuticle bands through which the adhesion-mediating secretion permeates via small canals. The secretion subsequently enters a larger storage reservoir before being received by a prominent sponge-like cuticle. The structural differences between the arolium and the euplantula consist of the number and length of the interdigitations spanning the hemolymph cavity, of the subdivision of the subcuticular reservoir by cuticle bands, and of the thickness of the sponge-like cuticle. The structural results are discussed with respect to the production of a chemically complex (emulsion-like) adhesive, its controlled release to the exterior, and the micromechanical properties of the cuticle of the pliable pad.

Keywords Adhesion · Gland · Insect · Cuticle · Tarsus

✉ Oliver Betz
Oliver.Betz@uni-tuebingen.de

[1] Institut für Evolution und Ökologie, Abteilung für Evolutionsbiologie der Invertebraten, Eberhard Karls Universität Tübingen, Auf der Morgenstelle 28, D-72076 Tübingen, Germany

Introduction

In the vast majority of insect orders, special tarsal morphologies have evolved that enhance their adhesive and frictional properties in the context of walking on various substrates. These adhesive structures are frequently described as attachment pads and can be found in most pterygote insects (Beutel and Gorb, 2001). While in rare cases such adhesive organs are associated with the tibia [e.g., the so-called Fossula spongiosa in reduviid bugs (Heteroptera); Weirauch 2007)], in most cases, the attachment pads are localized on the tarsus or pretarsus. According to Beutel and Gorb (2001), two distinct functional types, i.e., the smooth and the hairy tarsal adhesive pads, have evolved during the radiation of the insects more than once independently within the different orders. Although hairy adhesive pads can be found, for instance, in beetles (Coleoptera) (e.g., Stork 1980; Eisner and Aneshansley 2000; Betz and Mumm 2001; Betz 2002, 2003; Voigt et al. 2008; Bullock and Federle 2009; Geiselhardt et al. 2009, 2010) and flies (Diptera) (e.g., Bauchhenß 1979; Walker et al. 1985; Gorb 1998; Gorb et al. 2001; Niederegger et al. 2002), smooth adhesive pads are distributed over the orthopteran taxa (Kendall 1970; Henning 1974; Gorb et al. 2000; Gorb and Scherge 2000; Jiao et al. 2000), the dictyopterans (Roth and Willis 1952; Arnold 1974; Clemente and Federle 2008; van Casteren and Codd 2010), hymenopterans (e.g., Federle et al. 2002; Federle and Endlein 2004; Frantsevich and Gorb 2004), and numerous other orders (Beutel and Gorb 2001). The functionality of both the smooth and the

hairy attachment pads is based on the maximization of the effective contact area between the insect's feet and the substratum; this is achieved not only by the morphology of the pad (cf., Henning 1974; Jiao et al. 2000; Schwarz and Gorb 2003) but also by the presence of an adhesive fluid (e.g., Dewitz 1884; Federle et al. 2002; Vötsch et al. 2002; Langer et al. 2004; Drechsler and Federle 2006; Gorb 2007; Bullock et al. 2008; Dirks et al. 2010). Recent studies have confirmed the view that these adhesive fluids are complex emulsions composed of both hydrophobic and hydrophilic compounds (e.g., Reitz et al. 2015; Gerhardt et al. 2015, 2016; Betz et al. 2016). The emulsions can consist of lipid droplets in an aqueous fluid (Vötsch et al. 2002), or hydrophilic nano-droplets embedded in an oily continuous phase (Dirks et al. 2010). As reviewed by Betz (2010), numerous functional aspects of these highly complex mixtures have been considered. However, the chemical and micromechanical properties of the adhesion-mediating secretions are still poorly understood.

Several studies of the morphology of the adhesive pads in various insect orders have mostly focused on the composition of the adhesive pad cuticle, e.g., with an emphasis on its adjustment to diverse substrates, its frictional and adhesive performance, and the directional dependency of these structures (e.g., Gorb et al. 2000; Goodwyn et al. 2006; Clemente and Federle 2008). However, ultrastructural studies focusing on the cellular production of the adhesive fluid and its conveyance toward the tarsal pads surface are largely missing (see review in Betz 2010). With regard to adhesion structures employed in locomotion, such ultrastructural studies are available for the tarsal setae of coleopterans (Betz and Mumm 2001; Betz 2003; Geiselhardt et al. 2010), the pulvilli of aphids (Lees and Hardie 1988) and dipterans (Bauchhenß and Renner 1977; Bauchhenß 1979), the arolium of orthopterans (Kendall 1970) and mantophasmatodeans (Eberhard et al. 2009), and the euplantulae of orthopterans (Henning 1974).

The aim of the present study has been to elucidate the ultrastructure of the tarsal adhesive pads of the Madagascar hissing cockroach *Gromphadorhina portentosa* (Schaum, 1853) (Blattodea, Blaberidae) with special emphasis on the production and discharge of the adhesion-mediating secretion. This species was selected because recent studies had analyzed the chemical composition of its tarsal adhesion-mediating secretion and the adhesion and friction ability of both the arolium and the euplantula (Gerhardt et al. 2015, 2016; Betz et al. 2016, 2017). *G. portentosa* is easy to breed and ideally suited for the collection of adhesion-mediating secretion due to their large adhesion organs. According to the previous chemical analyses, the adhesive has a semi-solid consistency and contains mixtures of *n*-alkanes and methyl-branched alkanes in the range of C27–C33 (Gerhardt et al. 2015, 2016), together with peptides and (glycosylated) proteins ranging from 1 to 190 kDa in size (Betz et al. 2016). Recent studies of the attachment performance of the adhesive pads of *G. portentosa* have encompassed aspects such as global and local friction, local adhesion, surface roughness, and the influence of the tarsal adhesion-mediating secretion in its interaction with the compliant viscoelastic pad cuticle of the euplantulae (Betz et al. 2017).

The present contribution further complements these analytical and experimental approaches with respect to the specific morphology and ultrastructure of both the euplantulae and the arolia. The following questions have been addressed. Where is the tarsal secretion produced and where is it stored? And how is the secretion transported from the tissue where it is released to the surface of the smooth attachment pads? The analysis of these questions should contribute to our general understanding of the formation of the tarsal adhesive at the cellular level and its interaction with the pad cuticle in order for it to meet the functional requirements in the context of reversible attachment during locomotion.

Materials and methods

Animals

We examined adult cockroaches from our laboratory culture. The animals were kept in a terrarium that was structured with wooden branches and egg cartons. A layer of wood litter served as the substratum. The animals were fed with fresh fruit and dry cat food ad libitum. A diurnal light–dark cycle of 12 h during the day and 12 h during the night was chosen. The temperature (30 °C day, 22 °C night) and the relative humidity (20%) were kept constant. The weight differed between adult male and female cockroaches (6.43 ± 1.30 g and 8.10 ± 1.59 g, respectively; $n = 10$ individuals each, arithmetic mean ± standard deviation). As recommended by Zhou et al. (2015), only young animals (removed shortly after imaginal molting from our laboratory culture) with uniformly light-colored adhesive pads without any brown scars were selected for further analyses. In this study, we examined the adhesive organs of the pro-, meso- and metatarsus of both male and female individuals. As determined in preliminary tests, there is no sexual dimorphism with regard to the ultrastructure of the adhesive pads. Therefore, the transmission electron microscopic analyses, presented in this study, were performed using female cockroaches only.

Scanning electron microscopy (SEM)

The animals were tranquilized by using CO_2 and subsequently immersed into heated ethanol (70% v/v at 70 °C for 10 min) in order to achieve fast fixation of the sensitive tissue of the adhesion pads and thus to prevent the collapsing of the cuticle (cf., Piechocki and Händel 2007). The tarsi were then

removed and dehydrated through increasing concentrations of ethanol (70, 80, 90, 95, and 100% v/v per each 20 min; the last three steps were repeated twice) followed by critical-point drying (CPD) (Polaron 3100; Quorum Technologies, Laughton, UK). The samples were fixated on small cover glasses using a fast-curing two-component epoxy resin adhesive (UHU Zweikomponentenkleber Plus schnellfest; UHU, Bühl, Germany) that were in turn mounted on aluminum stubs covered with double-sided adhesive carbon tape and sputter-coated with a thin layer (approx. 20 nm) of gold (Emitech K550X; Quorum Technologies). In order to attain information about the inner organization of the adhesive organs, some samples were manipulated with a razorblade before being sputter-coated. Micrographs were obtained by viewing specimens with a Zeiss Evo LS10 SEM (Carl Zeiss, Oberkochen, Germany) at various acceleration voltages and magnifications.

Cryo-scanning electron microscopy (Cryo-SEM)

In order to prevent artifacts during cryo-fixation, fresh samples were frozen as rapidly as possible. We shock-frosted the legs in nitrogen slush (produced by applying a vacuum to liquid nitrogen) at −210 °C, thereby preventing the disruptive Leidenfrosts phenomenon. The frozen samples were either processed without further preparation or were freeze-fractured with a cold blade in the region of the adhesive organs. By the addition of a temperature gradient (Δt approx. 70 °C) between the copper sample holder and a cryogenic cold trap (temperature constant at −150 °C), the samples were freeze-substituted before they were sputter-coated with an approx. 15-nm-thick layer of gold. Preparation, freeze-substitution, and sputter-coating were conducted in the cryo preparation unit K1250X (Emitech, Ashford, UK). The samples were transferred to the SEM via an evacuated transfer unit and examined at a constant temperature of −150 °C in the Zeiss Evo LS10 SEM (Carl Zeiss).

Transmission electron microscopy (TEM)

Chemical fixation was performed at 0 °C unless otherwise noted. Specimens were tranquilized by using CO_2 before the tarsi were removed and submersed into the first fixation solution in order to avoid autolysis. This fixative corresponded to a modified Karnovsky's solution containing 33% formaldehyde, 1.66% glutardialdehyde, 4% sucrose, and 6.6 μM $MgSO_4$ diluted in 0.05 M 4-(2-hydroxyethyl)-1-piperazineethanesulphonic (HEPES) acid buffer at pH 7.25. The fixation time was either 60 min or 120 min at approx. 200 mbar. Samples were rinsed three times for 10 min in prechilled 0.05 M HEPES buffer and postfixed by using an aqueous solution of 1% osmium tetroxide in 0.05 M HEPES buffer. After being rinsed, the samples were dehydrated through a graded series of ethanol with steps of 30, 50, and 70% for 15 min, respectively. En bloc staining was conducted by using a saturated solution of uranyl acetate in 70% ethanol overnight at 4 °C. The following steps were performed at room temperature. Dehydration was continued in 10% steps (three times, 15 min each). Absolute ethanol was replaced by incubation in propylene oxide (two times, 15 min each). Samples were gradually infiltrated by incubation in AGAR LV (PLANO, Wetzlar, Germany) via a propylene oxide:resin mixture at ratios of 7:1, 3:1, 1:1, 1:3, for 1.5 h each, and then in fresh pure resin for 12 h on a rotary shaker, followed by a last incubation step in pure resin for 2 h. Specimens were finally embedded in epoxy resin in silicon molds. Polymerization was conducted at 60 °C for 48 h. Ultrathin sections (65 nm) were cut by using a Reichert Ultracut microtome (Leica-Jung, Vienna, Austria) and diamond knives (Diatome 45°; Biel, Switzerland). Ultrathin sections for transmission electron microscopy (TEM) were contrasted with ethanolic (50%) uranyl acetate for 30 min and lead citrate for 75 s. TEM studies were performed on a Siemens Elmiskop 1A transmission electron microscope (Siemens, Berlin, München, Germany) at 80 kV. Micrographs were taken on 6.5 × 9 cm plate negatives. Original negatives were scanned at high resolution (Epson Perfection V700 Photo; Epson, Japan) in 16-bit grayscale, and image processing was performed by using Adobe Photoshop (Adobe Systems, 2003). Image-processing included adjustments of the tonal range, manipulation of image size, bit depth reduction, and the merging of several images to give a panorama (cf. Bergmann et al. 2010; Bergmann and Heethoff 2012; Laumann et al. 2010).

Light microscopy

For analysis by light microscopy, semithin sections (0.5 μm) were generated from the same samples as those used to prepare ultrathin sections. The sections were placed on glass slides and stained with Stevenel's Blue (Del Cerro et al. 1980), which is routinely used in our laboratory for overview staining because of its simple implementation and easy to interpret results. The sections were examined with a Zeiss Axioplan light microscope. Images were processed in AxioVision 4.0 (Carl Zeiss).

Preparation of overview drawings

An overview diagram was created by summarizing the ultrastructural information of a representative panorama consisting of ten overlapping TEM images (×5000 magnification). Relevant structures such as cell organelles, vesicles, membrane structures, cell–cell contacts, and extracellular structures were drawn in an overview scheme,

scanned, and modified in Adobe Illustrator (Adobe Creative Suite CS4).

Results

External morphology of the tarsal adhesive structures

The general morphology of the tarsi of *G. portentosa* shows high similarity to the tarsi of other cockroaches (cf., Roth and Willis 1952; Arnold 1974; Clemente and Federle 2008; Zill et al. 2010; see also the descriptions of *G. portentosa* by van Carsteren and Codds 2010).

The tarsi of *G. portentosa* cockroaches are composed of five subsegments, termed tarsomeres (Ts_1–Ts_5), and the distal pretarsus (Pts) (Fig. 1a). The first tarsomere (Ts_1) is connected by a joint with the tibia, whereas each of the following tarsomeres are articulated with its preceding tarsomere, thus forming a flexible chain. Since the tarsomeres lack intrinsic muscles, the tarsal subsegments can be moved against each other only passively (cf., Zill et al. 2010). The unit is completed by the pretarsus that exhibits the strongest motion capability. The active movement of the pretarsus relative to the tarsomeres (flexing both the ungues and the arolium) is effected by the retractor unguis muscle (cf., Alsop 1978; Zill et al. 2010). Each of the tarsomeres, except for the fifth, possesses a smooth adhesive pad on its ventral side, the so-called euplantula (Fig. 1a, b). The trapeziform pad (called the arolium) associated with the pretarsus is positioned immediately between the claws (Fig. 1a, e). When viewed with the light microscope, the euplantulae and the arolium appear to be white and thus seem only weakly sclerotized and highly compressible. Whereas the ventral side of the arolium appears membranous, its dorsal side is protected by a sclerite plate. A longitudinal groove dividing the euplantulae of the individual tarsomeres into a right and a left lobe gradually increases from proximal to distal and is more pronounced in tarsomeres 3 and 4, which consist of a pair of pads rather than a single pad as is the case in tarsomeres 1 and 2 (Fig. 1a–c). Long sensory setae (sensilla trichodea, long type; length: 291.17 ± 74.47 μm, n = 10; measurements were performed within SEM images of one fore tarsus) are located on the lateral side of the euplantulae and also on the distal rim of the arolium. However, these sensory setae do not originate directly from the euplantulae but arise from sclerotized cuticle regions in the transition area to the soft cushions (cf. Fig. 1a–e). The surface of the euplantulae is mostly smooth and unstructured except for small areas of the euplantulae of the first four tarsomeres containing small grooves surrounding the paired mechanosensilla (sensilla trichodea, short type; length: 29.79 ± 9.45 μm, n = 10; measurements were performed within SEM images of one fore tarsus) (Fig. 1c, d). The spatial distribution of these mechanosensilla across the euplantula is similar for all the tarsomeres, and the distance between them and the central groove increasingly becomes smaller from lateral to distal. Additionally, in some analyzed individuals, close to the lateral margin of the euplantulae, the cuticle surface has an imbricate, hexagonal appearance (Fig. 1d). In those cases in which these structures are visible, the hexagonal pattern differs significantly in both clarity and localization (start of cuticular patterning). The ledges of these structures face in a medio-distal direction (diameter of hexagons: 4.07 ± 0.68 μm, n = 10; measurements were performed within SEM images of one euplantula of a fore tarsus).

The pretarsus (Fig. 1e) consists of two ventrally curved claws (ungues) that laterally flank the terminal arolium. The surface of the unpaired arolium bears a set of different structures (cf. Fig. 1f–h). On its most distal margin, the surface is characterized by an accumulation of digitiform projections (diameter: 4.51 ± 0.48 μm, n = 10; measurements were performed within SEM images of one arolium of a mesotarsus). The grooves formed between these knobs contain residues of the adhesion-mediating secretions (Fig. 1f). Further proximally, the surface of the cuticle is poorly structured. Narrow cuticular folds run parallel with a spacing of approximately 1 μm in a longitudinal direction (Fig. 1g). The surface of the most proximal part of the arolium is again more strongly structured. Here, the cuticle forms submicron-sized irregularities that lie close to each other, resulting in a surface structure resembling that of sandpaper (Fig. 1h).

Internal organization of the cuticle of the tarsal adhesive structures

Arolium

Figure 2 depicts SEM images of the arolium after CPD. The sagittal sections show the complex structure of the cuticle, which is formed by a network of chitin fibrils called rods of variable diameter and orientation, and which has been previously described for various insect species (e.g., Kendall 1970; Gorb et al. 2000; Goodwyn et al. 2006; Clemente and Federle 2008; Bennemann et al. 2014; Zhou et al. 2015). These chitin rods underlie both the transverse band of digitiform projections (Fig. 1e, f) and the mostly unstructured surface of the arolium (Fig. 1e, g), which is important for interactions with the substrate in the context of walking or climbing. The rods run almost vertically toward the ventral cuticle plane (angle: 91.28 ± 5.98°, n = 10; measurements were performed within SEM images of one arolium) and traverse the arolium from the ventral cuticle surface to deeper layers of the endocuticle in a slightly sigmoidal shape (Fig. 2b). In the ventral transition area to an external layer of the cuticle that is penetrated with pore canals, the rods branch into several smaller strands that taper off to form a more densely packed layer; this layer is

henceforth referred to as the layer of branched rods (diameter of the circular contact area of one single rod and its branches in the transition to the external layer of the cuticle (Fig. 2c): 12.25 ± 4.84 μm, n = 10; measurements were performed within SEM images of one arolium) (Fig. 2c; Lbr). The rods in the middle of the fibrillar endocuticle (layer of principal rods) have an average diameter of 2.26 ± 0.54 μm; n = 10, whereas in the layer of the branched rods, their diameter is 0.18 ± 0.03 μm; n = 10 (measurements were performed within SEM images of one arolium).

At higher magnifications, additional structures can be visualized that run almost perpendicular to the principal rods and interconnect these with variable spacing (Fig. 2c, d; Hc). Additionally, on the surface of the principal rods, structures can be detected that we have interpreted as residuals of a liquid filling the cavities of the cuticle (Fig. 2d; Mr). Because of the multitude of cavities in between the chitin fibrils, this type of endocuticle is frequently termed as spongy or sponge-like cuticle (e.g., Lees and Hardie 1988; Dixon et al. 1990; Clemente and Federle 2008; Scholz et al. 2008), even though the above described structure differs significantly from the structure found in natural sponges. However, since the so-called sponge-like cuticle functionally resembles natural sponges in their ability to store large amount of fluid, we decided to use this albeit slightly misleading terminology. In the arolium of *G. portentosa*, this characteristic cuticle layer has its maximum thickness (178.9 ± 5.8 μm, n = 10; measurements were performed within SEM images of one arolium) in the distal area covered with digitiform projections and continually decreases toward the proximal parts. The sponge-like endocuticle ends at the proximal boundary of the central and mostly unstructured cuticle area (cf. Figs. 1e, g and 2b). The endocuticle is covered by an epicuticle (thickness: 81.30 ± 42.9 nm, n = 10; measurements were performed within TEM images of one arolium), which constitutes the outer layer of the integument and thus the cuticula surface.

Euplantula

The sections of the euplantulae (Fig. 3a–d) and the freeze-fractures of this organ (Fig. 3e, f) also show a network of chitinous rods, which is characterized by numerous small cavities. Since the cuticle of the metatarsi was cut laterally, the rods run perpendicular to the section plane (Fig. 3c, d). On its ventral side, the cuticle is covered by a denser cuticle layer and the thin epicuticle (33.20 ± 6.18 nm, n = 10; measurements were performed within TEM images of one euplantula). On its dorsal side, the sponge-like cuticle is followed by a layered cuticle, which is succeeded by an inner part of the endocuticle. This inner layer is characterized by a large cavity that is traversed by numerous fibrils assembled into larger fibers (cf. Fig. 3c, d; Fb). However, these fibers are not visible in the light microscopic and the TEM images (cf. Fig. 4a–c). It can therefore be assumed that, during the dehydration required in the course of the SEM preparation, shrinking processes have led to numerous fine fibrils assembling into these large fibers. Thus, these structures are drying artifacts that probably do not represent the physiological condition. This assumption is further supported by the fractures of the native and shock-frozen euplantulae (Fig. 3e, f). These freeze-fractures show the transition between the sponge-like endocuticle and the inner parts of the endocuticle, which is characterized by large cavities filled with a homogeneous and granular matrix probably representing the emulsion-like adhesion-mediating secretion. Furthermore, the pore spaces within the sponge-like endocuticle are filled with this granular matrix (expected tarsal secretion).

The TEM images of the euplantula reveal the adhesion-mediating secretion that fills the cavities of both the inner and outer parts of the endocuticle. The secretion has a lower electron density than the chitinous components of the cuticle and exhibits a fine flocculent structure (cf. Fig. 4b–f). The mostly unstructured inner part of the endocuticle contains only a few chitinous structures and consists almost completely of a large secretion-filled cavity (Fig. 4a–c). In the proximity of the epidermis two denser and layered cuticle bands can be found, through which the secretion is able to pass via fine canals (Fig. 4a, b; iCb). Similarly, the regularly layered cuticular band in the transition area between the inner and the outer endocuticle also contains numerous pore canals (Fig. 4d). Further dorsally, the endocuticle is underlain by a single-layered epidermis, which is strongly invaginated (thickness: 14.39 ± 2.72 μm, n = 10; measurements were performed within light microscopic sections of one euplantula) (Fig. 4a, b). On the basis of these images, the entire cuticle can be considered a huge interconnected storage space for the secretion.

Ultrastructure of the glandular epidermal tissue

Euplantula

The epidermis that is associated with the euplantulae consists of a single (mono) cell layer and possesses numerous invaginations (Fig. 5a). These protrusions are formed by the inner parts of the endocuticle and are directed inward, i.e., into the hemolymph cavity of the adhesive pad (Fig. 5a, b). Some of these protrusions split into several terminations (Fig. 5a; double-headed arrow). Ventrally, the epidermis is followed by the cuticle layers described above, which are characterized by large cavities filled with the adhesion-mediating secretions (cf. Figs. 3, 4, 5). In contrast, the epidermal tissue of the dorsal side of the euplantula facing the strongly sclerotized cuticle is entirely unfolded and lacks cuticular cavities for the storage of an adhesion-mediating secretion. The epidermis is separated from the hemolymph by extracellular deposits that lie on the

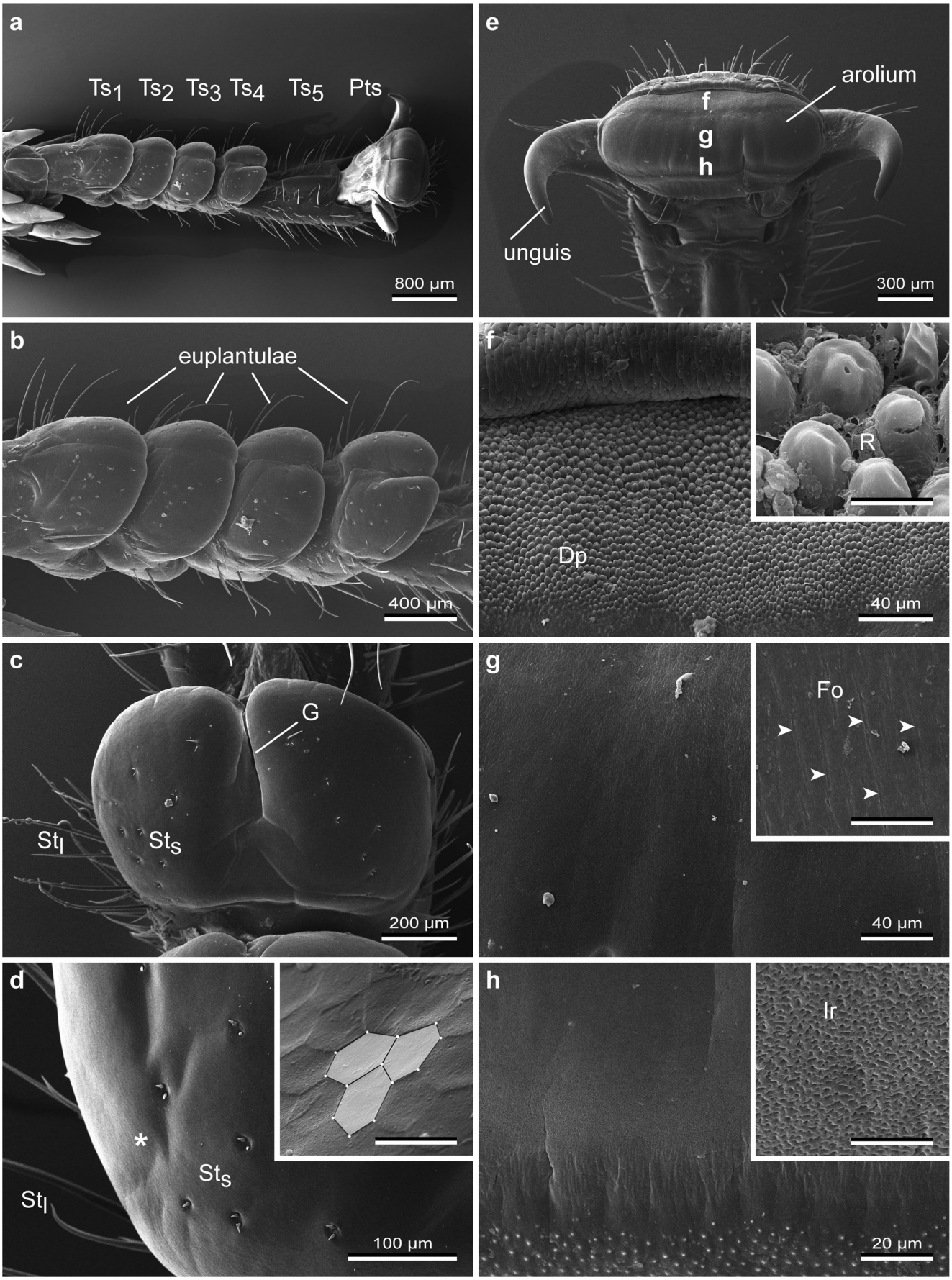
a
Ts1 Ts2 Ts3 Ts4 Ts5 Pts
800 μm
b
euplantulae
400 μm
c
G
Stl
Sts
200 μm
d
*
Sts
Stl
100 μm
e
arolium
f
g
h
unguis
300 μm
f
R
Dp
40 μm
g
Fo
40 μm
h
Ir
20 μm

◀ **Fig. 1** SEM images depicting the external morphology of the ventral pro- and mesotarsus of *G. portentosa* (male imago). The cockroach tarsus consists of five tarsomeres, of which the first four bear an euplantula (**a**–**d**), and a terminal pretarsus with an unpaired arolium inbetween the rigid ungues (**e**–**h**). The surface of the euplantulae appears generally smooth and unstructured but also exhibits areas covered with mechanosensilla (sensilla trichodea) located in small concavities of the cuticle (**c**, **d**). On the lateral margin of these pads, the cuticle surface sometimes has an imbricate appearance (**d**; *asterisk* indicates position at which hexagonal pattern begins). The ledges of these structures face medio-distally. The surface of the arolium is divided into three separate areas according to their surface structure indicated by (**f**), (**g**), and (**h**). The most distal part is characterized by a transverse band of digitiform projections (**f**), which is followed by a weakly structured area showing narrow, longitudinally oriented folds (**g**). At the proximal end of the arolium, an area can be found with tightly arranged irregularities in the submicron range (**h**). The *insets* in (**f**), (**g**), and (**h**) give a detailed view in higher magnification that is representative for the respective figure part and therefore characteristic for the corresponding position on the arolium displayed in (**e**). *Dp* digitiform projections; *Fo* folds; *G* central groove dividing the euplantula into two distinct lobes; *Ir* cuticular irregularities; *Pts* pretarsus; *R* residues of the adhesion-mediating secretion; St_l sensilla trichodea long type; St_s sensilla trichodea short type; Ts_1-Ts_5 tarsomeres 1–5; *white arrows* indicate position of cuticular folds; (**a**-**d**) fore tarsus (**e**–**h**) mesotarsus. *Scale bars of the insets* 5 μm

basal cell membrane and that appear as a connective tissue-like layer (cf., Figs. 5, 6h, i; Ctl). Embedded in this layer, tracheoles can be found that provide oxygen to the surrounding tissue (Fig. 6i; Tr). The connective tissue-like layer stretches from some of the epidermal protrusions into the interior, thus compartmentalizing the hemolymph cavity (Fig. 5a, b; Ctl). Whereas the deposits superimposing the epidermal tissue are not organized on a cellular basis, the same layer that merges into structures compartmentalizing the large internal volume is permeated by cells (cf., small and elongated nuclei in Fig. 5b; arrow).

The cytoplasm of the epidermal cells is densely packed with organelles, vacuoles, and membranous compartments. Its matrix has a moderate electron density and, because of numerous small inclusions, an inconsistent floccose appearance. Some of these inclusions have a higher electron density and appear as roughly isodiametric globules that, in this study, have been interpreted as free ribosomes. These particles are evenly distributed within the cytoplasm or associated with membrane components forming a rough-surfaced endoplasmic reticulum.

The surface of the apical cell membrane (facing the innermost cuticle layer) is organized in the form of a microvillus brush border, thus enormously increasing its surface (cf., Figs. 5c, 6a–e; Mv). In a laterad direction, the cell membrane establishes contact with the adjacent cell layer. In TEM images, the apical areas of these borders appear as a meandering interface, showing that the adjacent cells are strongly interconnected (cf., Figs. 5c, 6b, c). These interdigitations ensure tissue stability, especially in areas amenable to strong mechanical stress. The membranes of the contiguous epidermal cells are tightly connected to each other by septate junctions (see ladder-shaped structure in Fig. 6b; Sj) and desmosomes (Fig. 6h; Des). The surface of the membrane enclosing the basal cell pole is also strongly increased and forms a basal labyrinth (cf. Fig. 5c; Bl). The detailed TEM images frequently show pinocytic material transfer from the hemolymph into the cytoplasm along this membrane (cf., Figs. 5c, 6c; highlighted with arrowheads). Because of the strongly increased surfaces of both the apical and the basal cell membranes, the interface both to the hemolymph at the basal side of the epithelium and to the secretion-storing cuticular reservoir at its apical side is also strongly increased indicating a high membrane turnover.

The cells of the described epidermal epithelium are characterized by the presence of large, irregularly bordered nuclei that are mostly localized between the center and the basal area of the cytoplasm (cf., Figs. 5, 6; N). The cells are predominantly in interphase, as can be seen from the distribution of hetero- and euchromatin, and are associated with membrane lacuna that can be characterized as rough-surfaced endoplasmic reticulum (rER), since it is densely coated with ribosomes (cf. Figs. 5c, 6; rER). In most cells, membrane-enclosed and stacked cisterns of Golgi complexes can be identified within the cytoplasm (Fig. 6h; Gc). Furthermore, in all TEM images, the cells also contain numerous mitochondria that are often distributed all over the cytoplasm but that are, in most cases, preferably localized in the proximity of the apical cell pole or the basal labyrinth (Fig. 5c; Mi). In the TEM images, mitochondria can be found either in the form of slender tubular structures or ovate rounded cross-sections with an electron density similar to that of the darker regions (heterochromatin) of the nuclei. At higher magnification, the organelles can be classified as mitochondria of the tubular cristae type (Fig. 6g; Mi).

Additionally, numerous and diverse vesicle-like structures are distributed within the epidermal cells. Some of these vesicles are mainly lightly colored and large in diameter and are found predominantly in the proximity of the apical cell membrane. In contrast, other vesicles contain an irregular darker content that resembles the cytoplasm in terms of color and consistency (cf., Figs. 5c, 6; V). Moreover, multivesicular bodies (membrane-bound compartments with numerous small vesicles) can be found (cf., Figs. 5c, 6c; Mb). Various locations within the cytoplasm exhibit traces of the cytoskeleton, for example close to the nuclear membrane in the form of cross-sectioned microtubules (cf., Figs. 5c, 6f; Mt) or within the cytoplasm in the proximity of vesicles or vacuoles in the form of parallel-running microtubules (Fig. 6c, g; Mt).

Arolium

As shown in Figs. 7 and 8, the epidermal tissue of the arolium is similar to the epidermis of the euplantulae. The SEM and

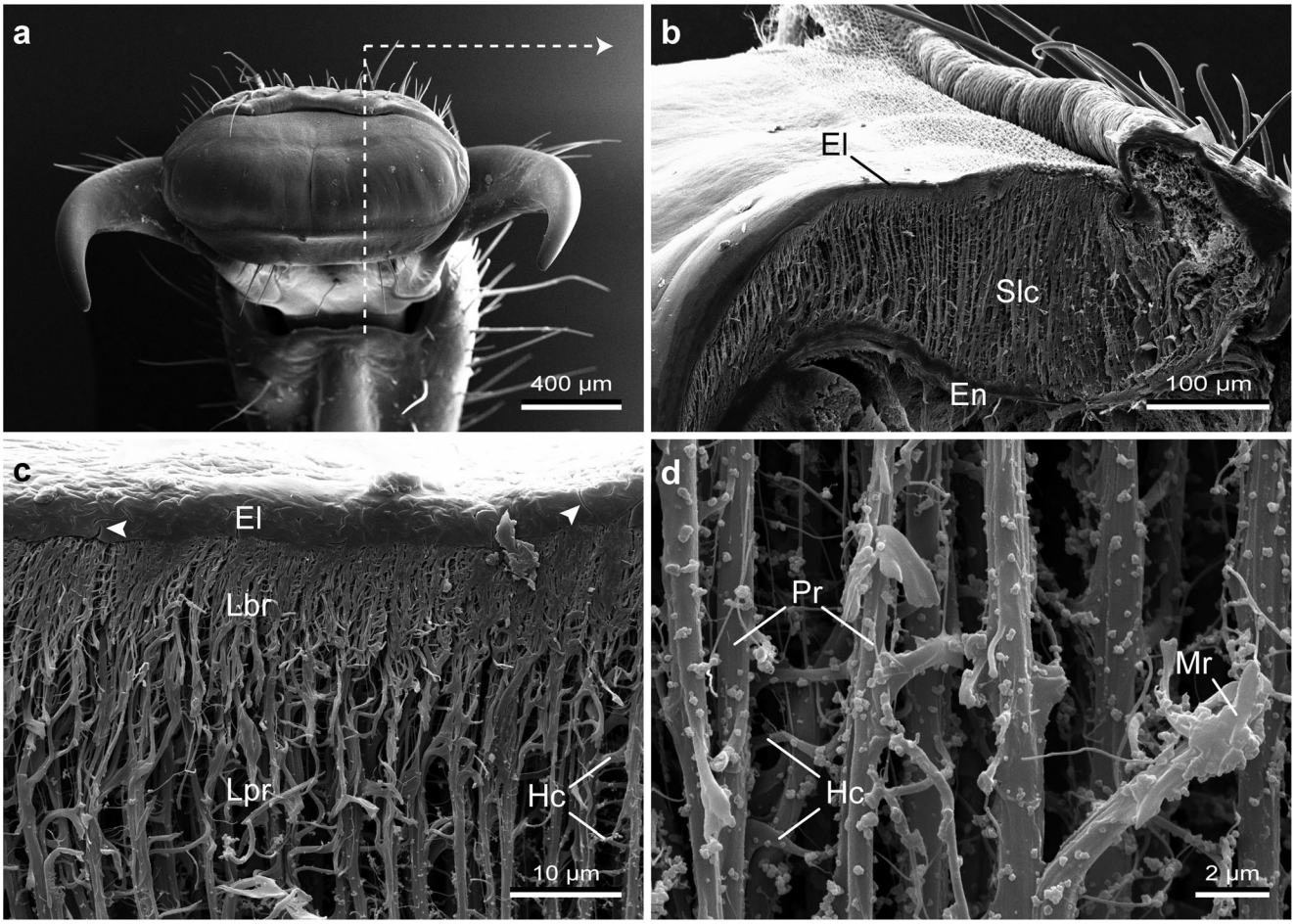

Fig. 2 SEM images showing the arolium of *G. portentosa* (metatarsus). The arolium of the cockroach was cut after critical-point drying by using a razor blade. The *dashed lines* in (**a**) ventral arolium designate the cutting plane of the sagittal section. **b** The endocuticle of the arolium is characterized by several parallel rods that enclose numerous gaps in between them. This sponge-like cuticle (*Slc*) is confined by a denser layer of the endocuticle (*En*) on its dorsal side and by an external cuticle layer (*El*) with pore canals (*white arrowheads* in **c**) and a thin epicuticle on its ventral side. **c** The principal rods of the middle and dorsal layers split up into several branches heading toward the ventral side. The branched rods (*Lbr*) thus form numerous contact points with the external cuticle layer (**b**, **c**). **d** At higher magnifications, the residues of a matrix (*Mr*) filling the cavity between the cuticular rods can be detected as material adherences on the principal rods. Additionally, horizontally oriented crosslinking structures (*Hc*) interconnect the principal rods. *En* endocuticle; *El* external cuticular layer and epicuticle; *Hc* horizontally orientated crosslinking structures; *Lbr* layer of branched rods; *Lpr* layer of principal rods; *Mr* matrix residuals; *Pr* principal rods; *Slc* sponge-like cuticle

light microscopic overview panels (cf. Fig. 7a, a', a") show invaginations of the inner cuticular layers into the hemolymph cavity on which the epidermis rests in the form of a single cell layer. In the upper left panel (SEM image; Fig. 7a), this can be explained by shrinking processes that occurred during the dehydration process and that led to the detachment of the cuticle bridges from the epidermal tissue. The light microscopic cross-sections (cf. Fig. 7a', a") show the transition between the sponge-like cuticle and the cuticle bridges that serve as a contact surface for the superimposing epidermis and as drainage structures for the adhesion-mediating secretion (Fig. 7a; Cu). Especially in deeper section planes (Fig. 7a"), the complexity of these structures, which fill out nearly the complete hemolymph space, becomes evident.

As in the euplantulae, the epidermal cell membrane of the arolium is folded both at the apical and at the basal cell pole, thus forming a microvillus brush border and a basal labyrinth (Fig. 7b–d; Mv). The lateral margins interacting with the adjacent cells are again strongly interconnected, thus forming interdigitations (Fig. 7e). As previously seen in the epidermal tissue of the euplantulae, areas of the basal labyrinth that are in contact with the hemolymph are superimposed by a connective tissue-like layer (cf. Figs. 7c, 8a, c; Ctl).

The cytoplasm of representative epidermal cells shown in the Figs. 7 and 8 is densely interspersed with organelles. As in the euplantulae, the large interphase nuclei are located centrally with respect to the cell width but lie closer to the basal part of the cytoplasm and are usually surrounded by a prominent

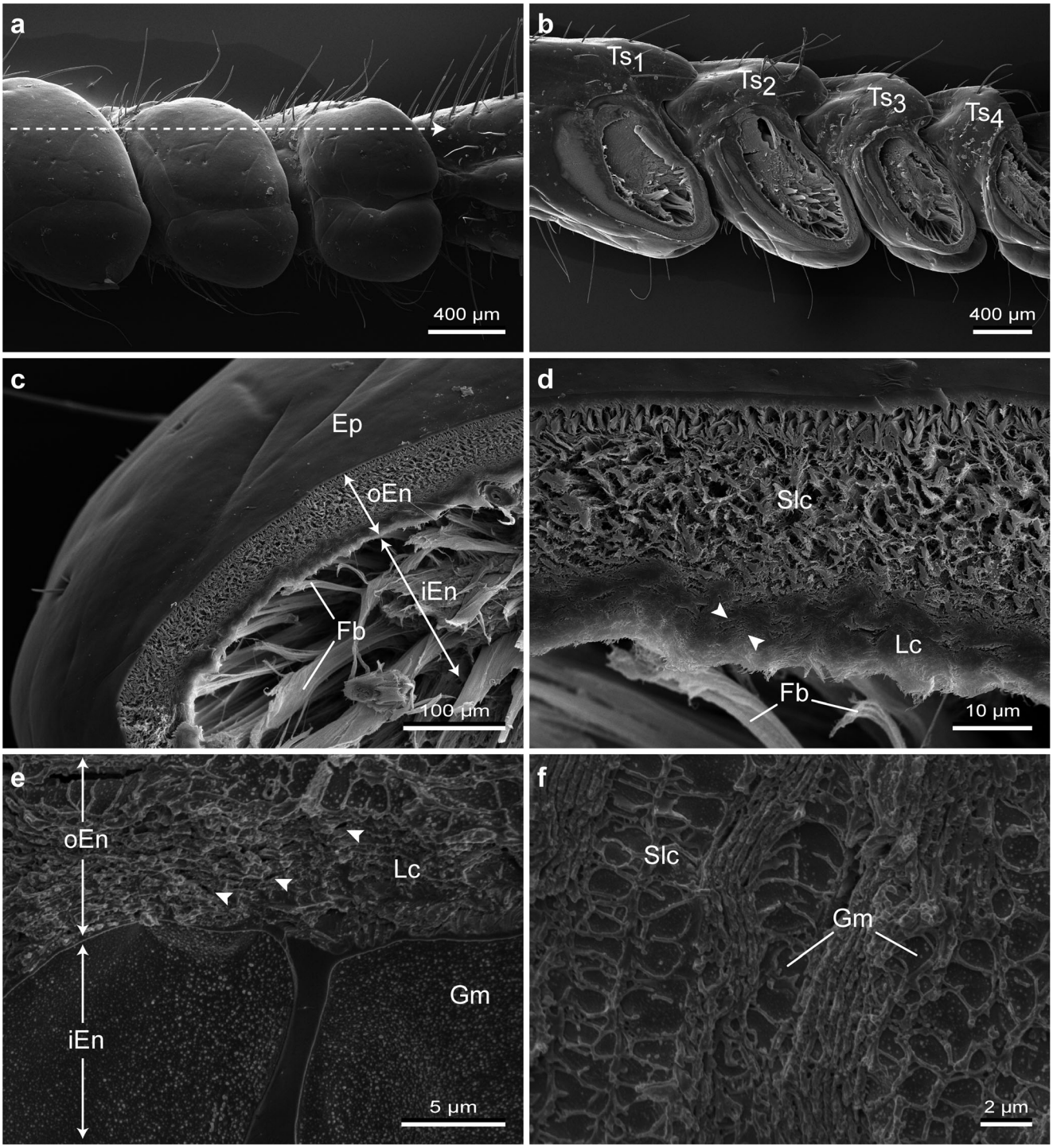

Fig. 3 SEM images showing the euplantulae of *G. portentosa* (metatarsus). Sagittal sections of critical-point-dried (**b**–**d**) and freeze-fractured (**e**, **f**) euplantulae. **a** The *upper left panel* shows the ventral surface of the adhesive pads (cf. Fig 1**a**–**c**); the following SEM images (**b**–**f**) focus on the cutting plane whose orientation is indicated by the *dashed line* in (**a**). **b**, **c** The cuticle of the euplantulae is subdivided into an outer part of the endocuticle (*oEn*), which is formed by chitinous rods enclosing numerous small cavities (sponge-like cuticle, *Slc*), and into an inner part of the endocuticle (*iEn*). A thin epicuticle constitutes the outermost layer of the integument. In the cut critical-point-dried samples (**b**–**d**), the inner part of the endocuticle is characterized by fiber bundles (*Fb*) supporting the cuticula. **e**, **f** The cryo-fractures representing the physiological state identify these fiber bundles as CPD-drying artifacts. In the freeze-fractures, the inner part of the endocuticle appears to consist of a large compartmented cavity that is filled with a uniform granular matrix (*Gm*). This matrix is considered the adhesion-mediating secretion and also fills the cavities of the sponge-like cuticle. *Ep* epicuticle; *Fb* fiber bundles; *Gm* granular matrix; iEn inner part of endocuticle; *Lc* layered cuticle; *oEn* outer part of endocuticle; *Slc* sponge-like cuticle; Ts_1–Ts_4 tarsomeres 1–4; *arrowheads* in (**d** **e**) indicate pore canals

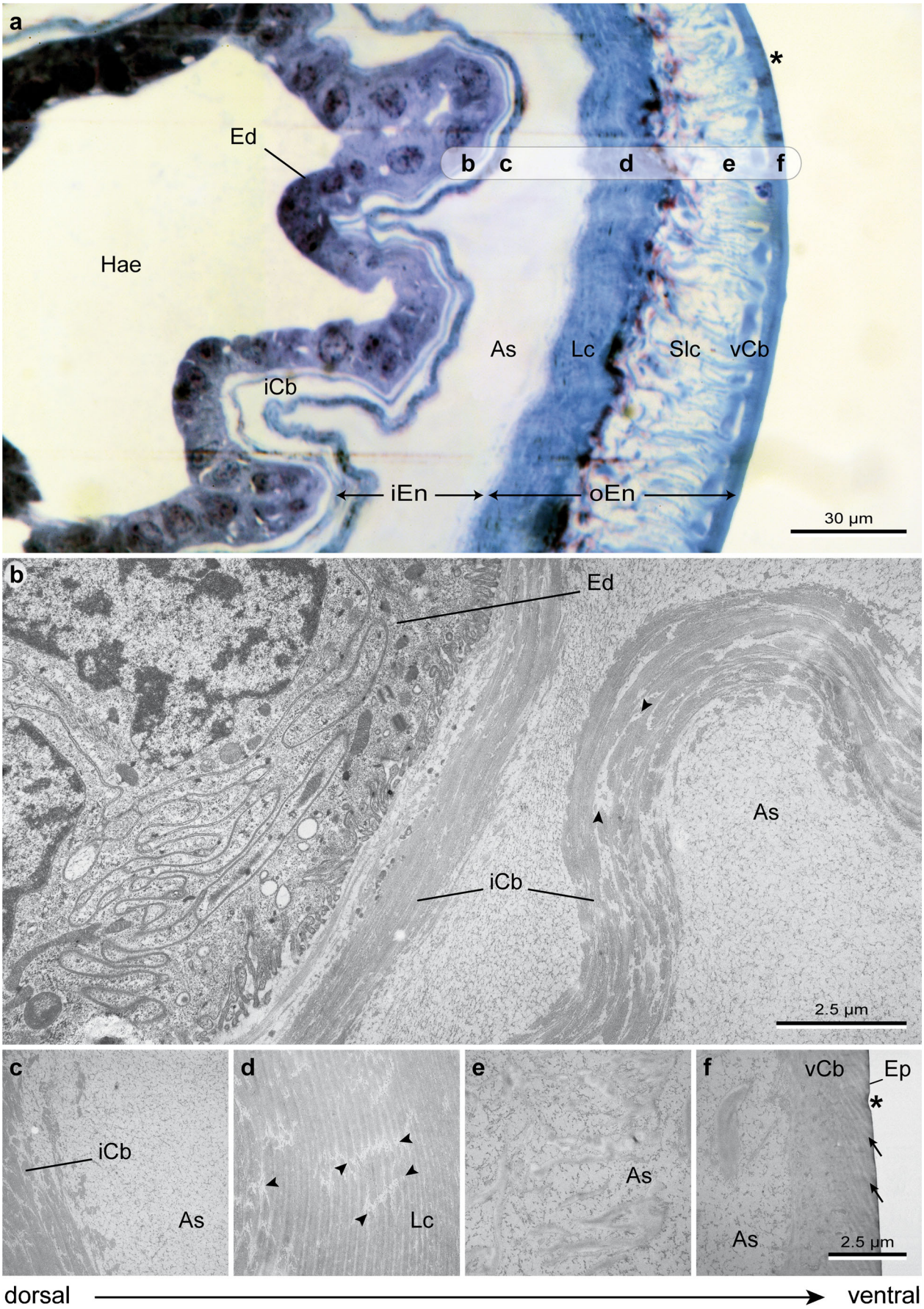
a
*
Ed
b c d e f
Hae
As
Lc
Slc
vCb
iCb
iEn
oEn
30 µm
b
Ed
As
iCb
2.5 µm
c
iCb
As
d
Lc
e
As
f
vCb
Ep
*
As
2.5 µm
dorsal
ventral

◀ **Fig. 4** Cross-sections through the euplantula of *G. portentosa* (protarsus). **a** The overview represents the general structure of the euplantula in a light microscopic thin section. The surface of the single-layered epidermis (*Ed*) is markedly enlarged by numerous invaginations. (**a**–**c**) The epidermis is then followed by the inner parts of the endocuticle (*iEn*), which contain a few chitinous structures which may serve as a huge storage cavity for the adhesion-mediating secretion (*As*). Close to the apical surface of the epidermis, two denser cuticle bands can be found with numerous pore channels through which the adhesion-mediating secretion can penetrate (*iCb*). The outer parts of the endocuticle (*oEn*) are located further ventrally. **d** This is subdivided into a (1) dorsally lying and regularly layered cuticle (*Lc*), which contains lamellae with the same orientation of microfibrils, and (2) a ventral region, which is characterized by chitinous rods forming a sponge-like structure (**a**, **d**–**f**). A thin epicuticle (*Ep*) (approx. 35 nm in thickness) constitutes the outermost layer of the cuticle (**f**). As adhesion-mediating secretion; *Ed* epidermis; *Ep* epicuticle; H*ae* hemolymph; *iCb* pair of inner cuticle bands; *iEn* inner part of endocuticle; *Lc* layered cuticle; *oEn* outer part of endocuticle; *Slc* sponge-like cuticle; *vCb* ventral cuticle band; *black arrowheads* indicate pore canals; *asterisks* the surface of the euplantula; *white box with small letters* in (**a**) the position of the detailed TEM images (**b**–**f**); *arrows* in (**f**) the termination of the pore canals)

rough-surfaced endoplasmic reticulum (Fig. 7f; rER). Golgi complexes can additionally be found (cf., Figs. 7b, 8b; Gc), and numerous mitochondria are broadly distributed over the cytoplasm but occur more frequently around the nucleus or rather at locations near the microvillus brush border and the interdigitations. This might be an indicator of extensive inter- or exocellular transport among these membrane structures, transport that is known to be energy-intensive (cf. Figs. 7, 8; Mi). The interior of the cells is tightly packed with vesicles of various sizes and electron density. The largest vesicles are usually characterized by their high electron transmissibility giving them an almost white appearance in the TEM images. The smaller vesicles generally appear darker in the images and sometimes are differentiated internally into a denser central and a paler cortical zone. Multilamellar bodies can frequently be found close to the cell membrane.

Discussion

To date, only a few studies have been conducted that have comprehensively elucidated the morphology of insect tarsal adhesive organs by combining studies on (1) the secretorily active tissues, (2) the cuticular structures that function in the storage, distribution, and release of the adhesion-mediating secretion, and (3) the external morphology of the adhesive organs and their interactions in the context of locomotion. The present study has aimed to examine all these aspects in order to provide an integrated overview of the structure and function of the adhesive organs. The investigation of the smooth adhesive tarsal organs of the Madagascar hissing cockroach in this study has elucidated the various hierarchically arranged structures and functions and their interdependences in the context of a complex organ system in greater detail.

First level of hierarchy: Ultrastructure of the epidermal cells

The epidermal cells of both the euplantulae (cf., Figs. 5, 6) and the arolium (cf., Figs. 7, 8) show a broad correspondence with respect to their ultrastructural composition, their connection to adjacent cells, and the organization of the interfaces that border the apical cuticular layers and the hemolymphatic cavity flanking the basal cell pole. Figure 9 summarizes the ultrastructural results of the electron microscopic analyses and is representative of the epidermal cells of both the euplantulae and the arolia. The following descriptions of these cells are highly characteristic for exocrine epidermal cells and therefore, in many aspects, reflect the literature regarding insect epidermal adhesive glands as reviewed in Betz (2010).

The cell membrane enclosing the cylindrical epidermal cells shows numerous adaptations emphasizing its exocrine function. The basal membrane is deeply infolded forming a prominent basal labyrinth (cf., Figs. 5c, 6h, 7c, 8a, c, 9). In some cases, the (extracellular) areas enclosed in between these membrane folds are permeated by cellular protrusions of adjacent cells (cf., Figs. 6a, c, 9). In some sections, a pinocytic material transfer along this membrane has been detected (e.g., Fig. 6h; highlighted with arrowheads). This is in accordance with Bauchhenß (1979), who describes similar structures in the pulvilli of *Calliphora erythrocephala* (Diptera, Calliphoridae) and who assumed that the enlarged membrane facilitates the transport of precursors of the secretion from the adjoining hemolymph toward the cytoplasm. Numerous other investigations have also verified the presence of a basal labyrinth within exocrine epidermal cells (e.g., Costa-Leonardo 2001; Müller et al. 2014). The apical cell membrane facing the cuticular storage reservoir is greatly increased. It is differentiated in the form of a microvillus brush border and consists of a great number of protrusions stacked very closely to one another; this is visible in the TEM images as long and slender extensions or as ovoid cross-sections (cf. Figs. 5, 6, 7, 9). This agrees with the results found in the literature (cf., Noirot and Quennedey 1974; Quennedey 1975; Bauchhenß and Renner 1977; Bauchhenß 1979; Lees and Hardie 1988; Costa-Leonardo 2001; Eberhard et al. 2009; Müller et al. 2014). Functionally, the deep invaginations of the microvillus border form an extensive reservoir for the secretion that either directly passes into the hollow shafts of the adhesive setae (Betz and Mumm 2001; Betz 2003; Geiselhardt et al. 2010) or permeates the cuticle layers in order to reach the surface of the smooth adhesive pads (cf. Figs. 5, 6, 7, 9). As described by Lees and Hardie (1988) and Betz (2003), the secretion within the reservoir appears sometimes to be inhomogeneous,

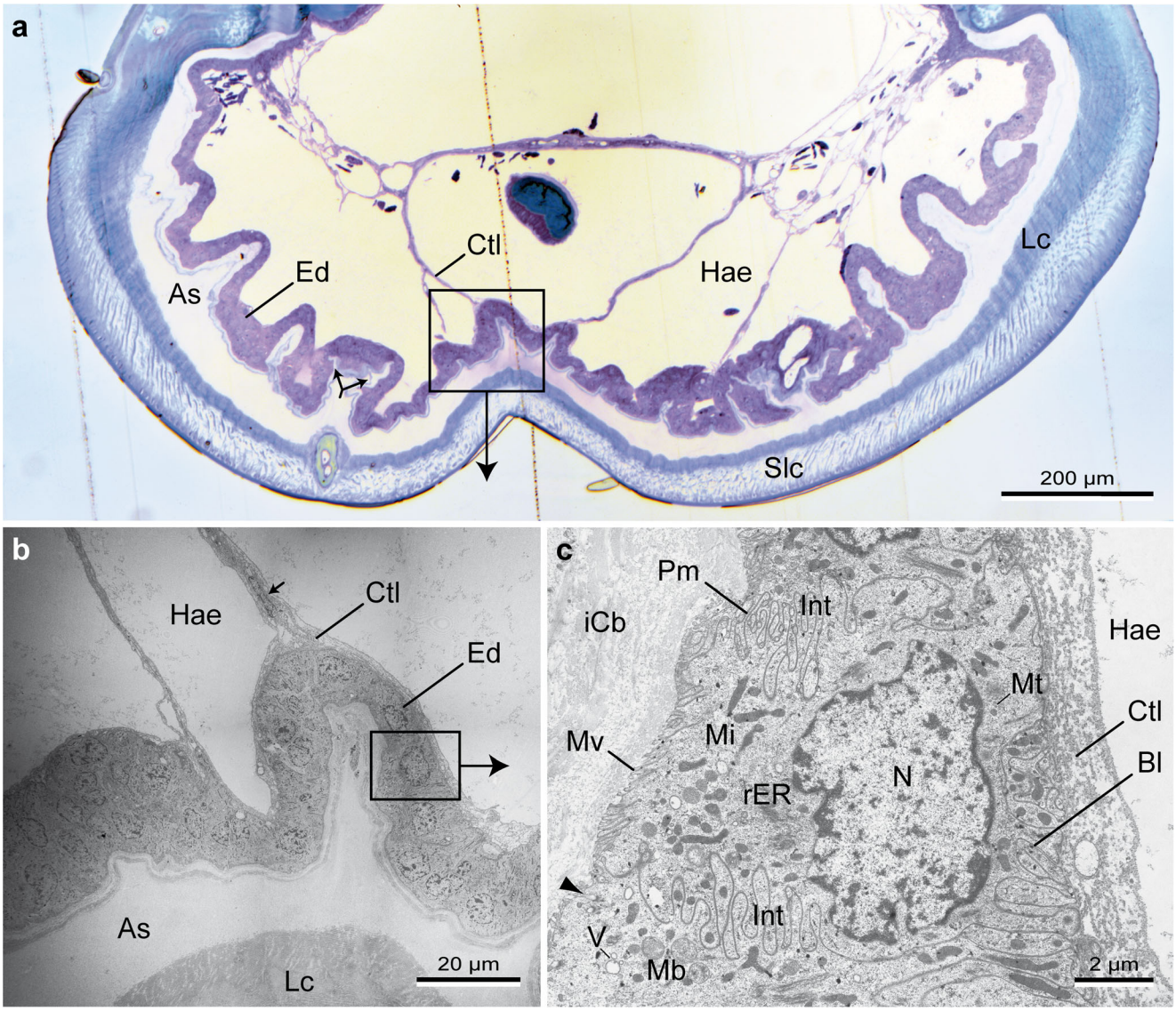

Fig. 5 Cross-sections through the euplantula (protarsus) of *G. portentosa* in light (**a**) and transmission electron (**b**, **c**) microscopic images showing a representative epidermal cell (**c**) and its localization both within the epidermis (**b**) and within the ventral part of an euplantula (**a**). The apical side of the epidermal cell is limited by a microvillus brush border that greatly enlarges the interface to the adjacent cuticle layers. Laterally, the cells are highly interconnected forming a complex network of interdigitations. At its basal pole, the epidermal tissue is bounded by the basal labyrinth on which an extracellular connective tissue-like layer is deposited. This layer additionally stretches from some of the epidermal protrusions into a dorsal direction and compartmentalizes the hemolymph cavity. The epidermal cells are densely packed with organelles (e.g., mitochondria, rough-surfaced endoplasmic reticuli, Golgi complexes, vesicles, multivesicular bodies, or components of the cytoskeleton) that are arranged around the large interphase nucleus. *As* adhesion-mediating secretion; *Bl* basal labyrinth; *Ctl* connective tissue-like layer; *Ed* epidermis; *Hae* hemolymph; *iCb* pair of inner cuticle bands; *Int* interdigitations; Lc layered cuticle; *Mb* multivesicular bodies; *Mi* mitochondria; *Mt* microtubules; *Mv* microvilli; *N* nucleus; *Pm* plasma membrane; *rER* rough-surfaced endoplasmic reticulum; *Slc* sponge-like cuticle; *V* vesicle; *double-headed arrow* in (**a**) indicates dichotomous branching of a protrusion; *arrow* in (**b**) an elongated nucleus within the connective-tissue-like layer; *arrowhead* in (**c**) a vesicle fusing with the apical membrane

forming a matrix that contains fibrils or flocculent structures. This is in agreement with the results from the TEM analysis presented in this study (e.g., Fig. 7b–d). A vesicle that fuses with the apical membrane and thus releases its content into the cuticular reservoir is shown in Figs. 5c and 6c. Such exocytic processes have also been detected by Bauchhenß and Renner (1977), Bauchhenß (1979), and Eberhard et al. (2009) in other adhesive attachment organs of insects. The membrane bordering the lateral sides of the epidermal cells at the interface to the adjacent cells is variously arranged from apical to basal. In the apical area, the cell membrane appears as a meandering interface interconnecting the adjoining cells (cf., Figs. 5c, 6b, c, 7b–e, 8b, 9). Such interdigitations are characteristic of epidermal exocrine tissue and have also been described in the studies

of Bauchhenß and Renner (1977), Lane et al. (1977), Costa-Leonardo (2001), and Serrão et al. (2008). The authors discuss the function of these membrane structures in enhancing the mechanical stability of the cell-cell contact. This is also evidenced by the high density of septate junctions localized within the areas of the interdigitations (e.g., Fig. 7e; cf., Lane et al. 1977; Costa-Leonardo 2001; Serrão et al. 2008). In studies focusing on intercellular junctions in the insect central nervous system, the large number of junctions has great importance with regard to the controlled intercellular exchange of substances. Here, the interdigitations were considered to enlarge the surface of the cell membrane in order to maximize the total amount of junctions per unit area of luminal surface (cf., Claude and Goodenough 1973; Lane et al. 1977). In the epidermal cells analyzed in our study, septate junctions have most frequently been found in association with the interdigitations, but also occur in a smaller number further basally. Even further basally, after approximately one-third of the longitudinal extent of the cell membrane, no more septate junction can be found, which agrees with the results of Bauchhenß (1979), Eberhard et al. (2009), and Costa-Leonardo (2001). At the basal cell pole, the adjoining membranes are connected with each other by desmosomes (Fig. 6h; Eberhard et al. 2009).

The cytoplasm of the epidermal cells of both the euplantulae and the arolia has a comparable electron density. According to Bauchhenß (1979) and Lees and Hardie (1988), the electron density of the exocrine cells is higher than that in other epidermal tissues. Additionally, exocrine cells are densely interspersed with organelles, vesicle-like structures, and membranous compartments. Because of numerous small inclusions, the matrix has an inconsistent floccose appearance (cf. Figs. 6, 7, 8). A large part of the cytoplasm is occupied by the large nuclei that are several micrometers in diameter. The nuclei are mostly positioned in the basal half of the epidermal cells, thus giving them a polar structure (cf. Figs. 5, 7, 8, 9). This is in accordance with Kendall (1970), Bauchhenß (1979), Betz and Mumm (2001), Betz (2003), and Eberhard et al. (2009). Clump-like heterochromatin aggregations are deposited within the light-colored nucleoplasm (cf., Bauchhenß 1979) indicating that the cells are in interphase. According to Betz (2010), secretorily active cells are characterized by their large number of mitochondria, and indeed, the epidermal cells of *G. portentosa* clearly provide evidence of this. Mitochondria of the tubular cristae type (cf., Figs. 6g, 7f) are distributed all over the cytoplasm but, in most cases, are preferably localized in proximity to the nucleus, the apical cell pole, or the basal labyrinth (cf., Figs. 5, 6, 7, 8). As illustrated in the TEM images, branched membrane lacuna of the endoplasmic reticulum originating from the nucleus traverse the cytoplasm. They can cover large areas of the cytoplasm and are densely coated with ribosomes, an indicator of active protein biosynthesis (cf. Bauchhenß and Renner, 1977; Bauchhenß, 1979; Lees and Hardie, 1988; Costa-Leonardo, 2001; Eberhard et al., 2009). Furthermore, Golgi complexes could be found in both epidermal tissues.

Apart from these organelles, the epidermal cells are characterized by their abundant secretion vesicles that vary in size and electron transmittance. The largest vesicles found in the TEM images are lightly colored and often located in proximity to the microvillus border. Additionally, numerous smaller and electron-denser vesicles are distributed over the cytoplasm but are preferably localized close to the apical membrane. The large number and diversity of vesicles is characteristic of many exocrine epidermal gland tissues as described in Bauchhenß and Renner (1977), Bauchhenß (1979), Lees and Hardie (1988), Betz and Mumm (2001), Betz (2003), and Eberhard et al. (2009). Moreover, multivesicular (cf., Bauchhenß 1979) and multilamellar bodies (cf., Bauchhenß 1979; Costa-Leonardo 2001) can be found in these cells (cf., Figs. 6c, 8).

Ultrastructure of the exocrine epidermis cells with respect to the composition of the adhesion-mediating secretion

So far, little is known about the composition of the tarsal adhesion-mediating secretions of insects, and only a few of these secretions have been analyzed in molecular detail (reviewed in Betz 2010). However, these secretions are known to consist of both a hydrophilic and a hydrophobic phase, thus forming a complex and heterogeneous emulsion (e.g., Vötsch et al. 2002; Dirks et al. 2010; Dirks 2014). However, the modes of action of their individual components and their chemical and micromechanical functions are still poorly understood (Betz 2010). In the context of locomotion, the studies of Ishii (1987), Kosaki and Yamaoka (1996), Vötsch et al. (2002), Betz (2003), Geiselhardt et al. (2009, 2010), Reitz et al. (2015), Gerhardt et al. (2015, 2016), and Betz et al. (2016) focus in particular on the analysis of insect tarsal secretions. For *G. portentosa*, Gerhardt et al. (2015, 2016) have been able to demonstrate the existence of various *n*-alkanes and methylbranched alkanes on the tarsal surface of the cockroach by using both solvent extraction and solid phase micro extraction (SPME) followed by gas chromatography coupled to mass spectrometry (GCMS). In order to identify the hydrocarbons that are important for the active adhesion principle and thus are different from the hydrocarbon pattern generally found on the cuticle surface, these results have been statistically compared with control samples collected from the tibiae. The detected *n*-alkanes and methylbranched alkanes in the range of C27-C33 are abundant on both the tarsal and the tibial surfaces, and, thus, no special hydrocarbons can be attributed exclusively to the adhesion-mediating secretion. Nevertheless, significant differences between the tarsi and tibiae in terms of the absolute abundances of hydrocarbons have been revealed. Unless the specimens are sampled with SPME

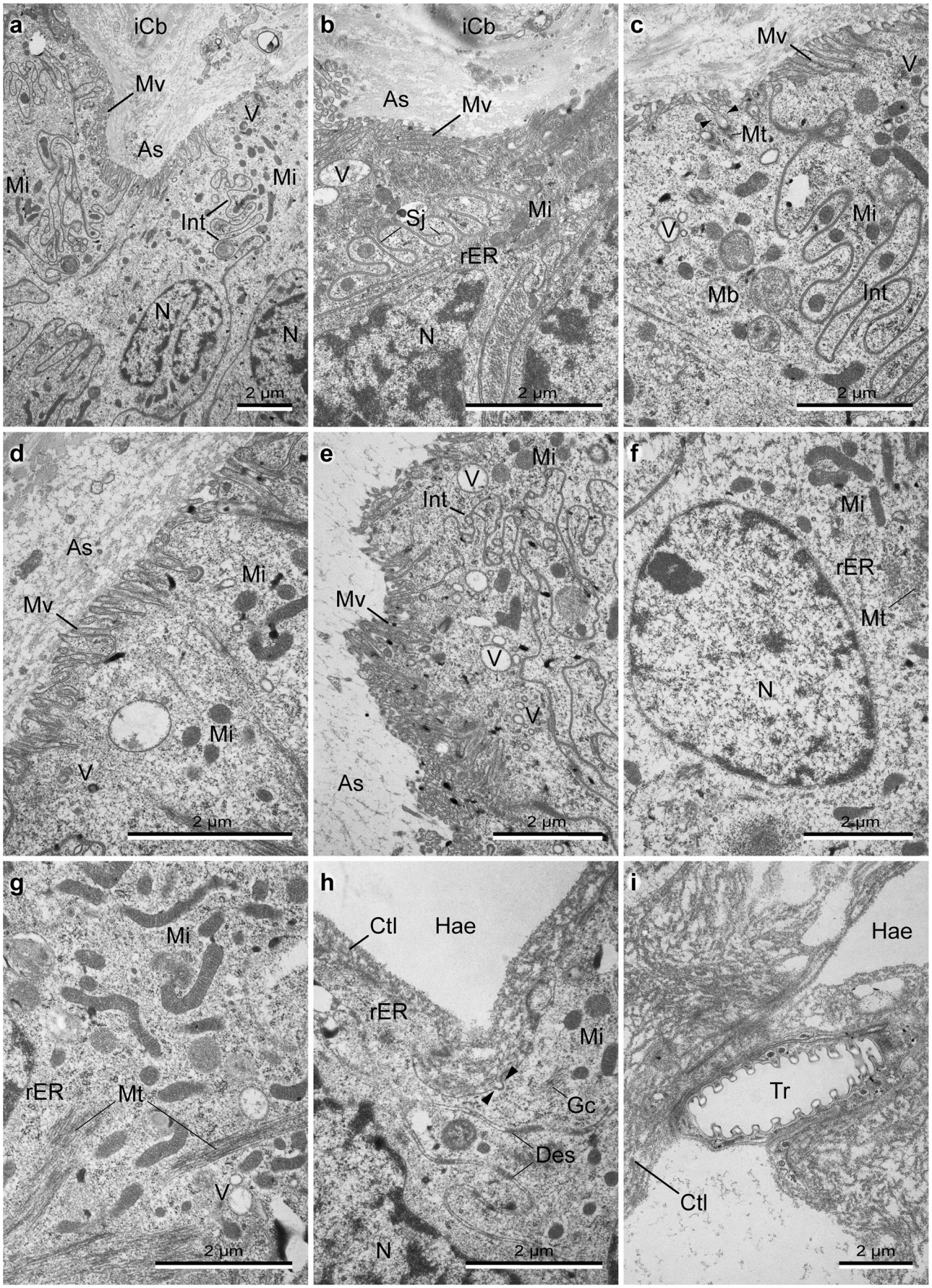
a
iCb
Mv
V
As
Mi
Mi
Int
N
N
2 μm
b
iCb
As
Mv
V
Sj
Mi
rER
N
2 μm
c
Mv
V
Mt
Mi
V
Mb
Int
2 μm
d
As
Mi
Mv
Mi
V
2 μm
e
Mi
V
Int
Mv
V
V
As
2 μm
f
Mi
rER
Mt
N
2 μm
g
Mi
rER
Mt
V
2 μm
h
Ctl
Hae
rER
Mi
Gc
Des
N
2 μm
i
Hae
Tr
Ctl
2 μm

◀ **Fig. 6** Detailed TEM images of crosssections through the euplantula of *G. portentosa* (protarsus). **a**–**e** regions from the apical, (**f**, **g**) from the central, and (**h**, **i**) from the basal part of representative epidermal cells. A detailed description of these structures is provided in the text. The *arroweads* in (**c**) indicate a vesicle fusing with the apical membrane to release its content into the cuticular reservoir (exocytosis). *Arrowheads* in (**h**) highlight the uptake (pinocytosis) of hemolymphatic content at the basal membrane into the cell. *As* adhesion-mediating secretion; *Ctl* connective tissue-like layer; *Des* desmosome; *Gc* Golgi complex; *Hae* hemolymph; *iCb* pair of inner cuticle bands; Int interdigitations; Mb multivesicular bodies; *Mi* mitochondria; *Mt* microtubules; *Mv* microvilli; *N* nucleus; *rER* rough-surfaced endoplasmic reticulum; *Sj* septate junction; *Tr* tracheole; *V* vesicle; *arrowheads* in (**c**) exocytosis; *arrowheads* in (**h**) pinocytosis

techniques, the abundance of hydrocarbons located on the tarsi is smaller (about three-fold) compared with that of the tibiae. If the specimens are sampled by solvent extraction (heptane), the result is inverted, i.e., more hydrocarbons are found on the tarsi than on the tibiae. These contradictory results can be explained on the basis that the sampling method of SPME fibers only considers the hydrocarbons exposed on the surface, whereas solvent extraction also captures the hydrocarbons that are stored together with the adhesion-mediating secretions within the sponge-like cuticle reservoir (Gerhardt et al., 2015).

In contrast to the above-mentioned studies, Betz et al. (2016) exclusively focused on the proteinaceous fraction (hydrophilic compounds) of the secretion in *Schistocerca gregaria* (Orthoptera, Acrididae) and *G. portentosa*. They used a combination of methods, including combined Fourier transform infrared spectroscopy, sodium dodecyl sulfate polyacrylamide gel electrophoresis (SDS-PAGE), and matrix-assisted laser desorption/ionization mass spectrometry (MALDI-TOF MS) analyses for protein mass detection. All these different approaches revealed the presence of peptides/proteins in the secretion. Using SDS-PAGE, they detected 17 different peptide/protein bands in the range of 7.9–190.5 kDa in samples taken from the tarsi and tibiae (negative control) of *G. portentosa*. One of these bands (157.6 kDa) was present in the tarsal secretion only, whereas no unique bands were detected for the tibia sample (see tables in Betz et al. 2016). With MALDI-TOF MS (considering only peptides with masses >1 kDa and signal to noise ratios >5), they could detect 48 different peptides (36 in the tarsal secretion, 21 in the femur and tergite controls) in the range of 1–11 kDa in both the tarsal secretion and the tibia sample. Each of these candidates was found in at least two independent measurements (see tables in Betz et al. 2016). The regular intervals of the detected peptide fragments of about 160 Da in the range between 9960 and 12,000 Da are indicative of glycosylated proteins that might differ in one saccharide monomer or dimer.

The results of the above-mentioned chemical analysis match well with the ultrastructural findings presented in this study. As to the hydrocarbons found in Gerhardt et al. (2015, 2016), the epidermal exocrine cells should provide evidence for the production and excretion of lipoid substances in their fine structure. The TEM images provided in Figs. 5, 6, and 7 clearly support this. The largest and most electron lucent vesicles found in the cytoplasm, especially in proximity to the apical cell pole, show characteristics of their lipophilic content, with regard to their size and coloration. As described in Fawcett (1981), the color of lipid inclusions found in TEM images varies greatly depending on the employed fixation and staining techniques. Following the fixation methods applied in this study, the inclusions appear as bright and electron transmittant structures. This is also confirmed by ultrastructural studies of the wax glands in bees (e.g., Hepburn et al. 1991; Cassier and Lensky 1995); these glands are known for their production of saturated hydrocarbons in the range of C25–C33. The presence of peptides/proteins in the tarsal adhesion-mediating secretion found by Betz et al. (2016) is also compatible with the fine structure of the exocrine epidermal cells. As shown in Figs. 5, 6, 7, 8, these cells contain numerous and prominent endoplasmic reticuli that are densely covered with ribosomes. This strongly indicates intense protein biosynthesis. We can reasonably assume that the smaller and electron-denser vesicles found in the TEM images contain proteinaceous components that are transported and secreted to the apical secretion reservoir.

Second level of hierarchy: Epidermal tissue functioning as glandular epithelium

As shown in Figs. 5 and 7, the exocrine epidermal cells are organized in a single-layered epithelium. This glandular epithelium is situated on cuticular protrusions and is strongly invaginated toward the hemolymph cavity (cf., Henning 1974; Eberhard et al. 2009), thereby strongly increasing the surface of the excretory epithelium. This applies in particular to the epidermis of the arolium (Fig. 7), which spans almost all of the interior of the adhesive organ, but also holds for the epidermis of the euplantulae, which is infolded to a lesser extent. The advantage of this morphology might have various aspects. First of all, the enlarged surface offers more space for excretory cells, thus increasing the amount of adhesive that can be secreted per time. Secondly, as described above, the cuticle of the adhesive organs interacting with the substrate surface is not sclerotized and thus has a soft and compliable appearance. This also means that during locomotion, the adhesive organs are regularly compressed and therefore mechanical stresses arise within these structures. Whereas the soft cuticular structures are robust and unsusceptible to damage caused by these mechanical stresses, the epidermal tissue could easily become compromised. However, by deformation of its infoldings, a pleated epidermal tissue can accommodate such stresses much better than a flat one. Thirdly, the meandering interdigitations of the cell membranes at the

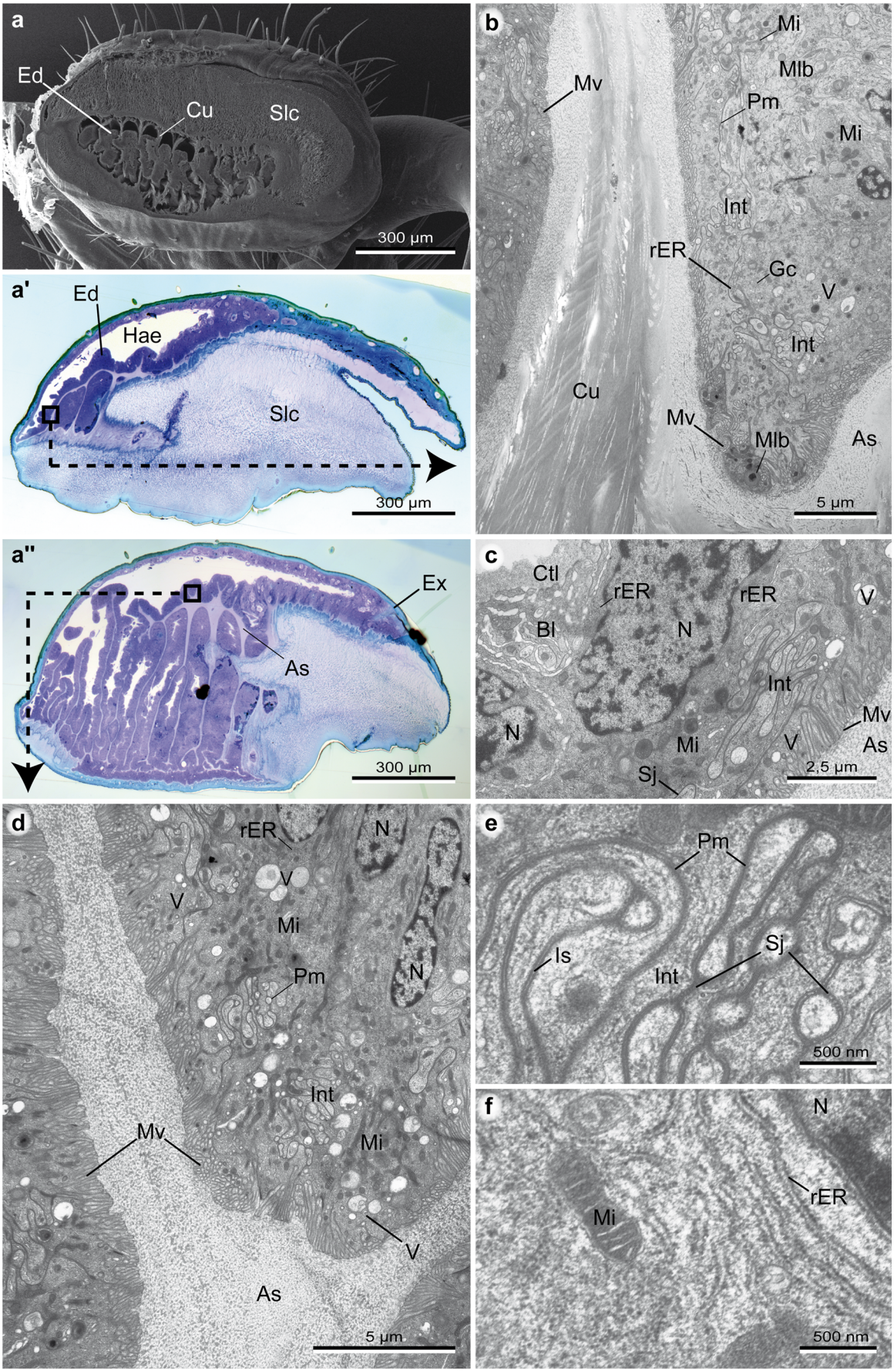
a
Ed
Cu
Slc
300 µm
a'
Ed
Hae
Slc
300 µm
a''
Ex
As
300 µm
b
Mi
Mlb
Mv
Pm
Mi
Int
rER
Gc
V
Int
Cu
Mv
Mlb
As
5 µm
c
Ctl
rER
rER
V
Bl
N
Int
Mv
N
Mi
V
As
Sj
2,5 µm
d
rER
N
V
V
Mi
Pm
N
Int
Mv
Mi
V
As
5 µm
e
Pm
Is
Sj
Int
500 nm
f
N
rER
Mi
500 nm

◀ **Fig. 7** Cross-sections through the arolium of *G. portentosa* (mesotarsus). **a** Overview of the entire cut in SEM and (**a'**, **a"**) light microscopic images (protarsus). Invaginations of the cuticle superimposed by epidermal tissue stretch deeply into the hemolymph cavity. The cuticle serves both as a contact surface for the epidermal cells and as canal-like structures for draining the adhesion-mediating secretion. The *upper right panels* (**b**, **c**) show details of the ultrastucture of the epidermal cells, whose localization is indicated by the *dashed line* in (**a'**). The *lower panels* (**d**–**f**) show details of the epidermal tissue, from a deeper cutting plane. The orientation of these images is indicated by the *lower dashed line* in (**a"**). The TEM images of the *right* and *lower panels* (**b**, **c** and **d**–**f**) provide information about the ultrastructure of the epidermal cells and reveal that the epidermal cells are strongly involved in an exchange with the hemolymph (basal labyrinth) and with the cuticle (microvillus brush border). Together with the large number of mitochondria and vesicles, this is indicative of the glandular function of these cells. *As* adhesion-mediating secretion; *Bl* basal labyrinth; *Ctl* connective tissue-like layer; *Cu* cuticle; *Ed* epidermis; *Ex* exocuticle; *Gc* Golgi complex; *Hae* hemolymph; *Int* interdigitations; *Is* intercellular space; *Mlb* multilamellar bodies; *Mi* mitochondria; *Mv* microvilli; *N* nucleus; *Pm* plasma membrane; *rER* rough-surfaced endoplasmic reticulum; *Sj* septate junction; *Slc* sponge-like cuticle; *V* vesicle

interface of two adjacent cells together with the basal desmosomes improve both the intercellular coherence and the resilience against mechanical stresses.

In the literature, three different types of epidermal exocrine gland structures are described (cf., Noirot and Quennedey 1974, 1991; Quennedey 1975, 1998; Betz 2010). According to Noirot and Quennedey (1974), the presence of a cuticle covering the gland tissue is characteristic of all three classes of epidermal glandular cells. They can be classified in accordance with their cell structure, their cuticle, and the manner of release of the secretions through the cuticular barrier toward the exterior. In *G. portentosa*, the exocrine cells associated with the tarsal adhesive organs belong to class 1 cells, representing the simplest type. They are defined by their fine structure (cf., descriptions in "First level of hierarchy") and the absence of specialized release structures. The exocrine cells that typically are cylindrical in shape thus secrete their products directly into the cuticle or a reservoir between the cuticle and the epidermal tissue. As no canal-like structures are present, the secretion has to penetrate the overlying cuticle barrier, which is therefore often perforated by pores. As reviewed in Betz 2010, all studies focusing on insect tarsal adhesive systems have described clusters of class 1 cells integrated into glandular epithelia. In some coleopterans, additional class 3 glands have been documented, whose function has not as yet been clarified.

Third level of hierarchy: Specialized cuticle formation related to storage and distribution of the adhesion-mediating secretion

The cuticle of both the arolia and the euplantulae has some special adaptations that make possible (1) the uptake of the adhesion-mediating secretion produced in the underlying exocrine epidermal tissue, (2) the storage and distribution of the secretion within its internal cavities, and (3) the forwarding of the secretions toward the exterior cuticle surface. Therefore, its morphology largely differs from the general structure of the insect cuticle, which, for example, can be found on the dorsal sides of the adhesive organs and which functions here as a "lightweight skeleton" (Vincent and Wegst 2004) protecting the vulnerable inner structures. Whereas the general cuticle is differentiated into an outer strongly sclerotized exocuticle and an inner soft endocuticle, a sclerotized exocuticle is absent in the cuticle of the adhesive organs which is in contact with the substrate surface. Another difference is that the soft cuticle of the adhesive organs is much thicker than the cuticle found in other parts of the insect surface (cf. Lees and Hardie 1988; Schwarz and Gorb 2003; Eberhard et al. 2009). This difference is most pronounced in the arolia, where the dimension of the soft cuticle exceeds that of the sclerotized cuticle typically more than ten times. In the euplantulae and the arolia, the innermost-lying parts of the cuticle, which are in contact with the epidermis, form protrusions reaching toward the hemolymph cavity in order to enlarge the surface area on which the epidermis rests. Between these protrusions and the microvillus border of the epidermal cells, a subcuticular gap or void can be found that has previously been denoted as a reservoir for adhesion-mediating secretions (e.g., Bauchhenß 1979; Eberhard et al. 2009; Betz 2010).

Our findings concerning the internal organization of the euplantula with respect to the storage spaces and the associated cuticle (cf. Fig. 4) are summarized in Fig. 10. After its release from the epidermal layer, the adhesion-mediating secretion has to permeate two layered cuticle bands (cf. Fig. 10; iCb) in order to enter a second large reservoir positioned within the inner part of the endocuticle. As shown in Fig. 4b, c, these bands are permeated by numerous dilated pore canals (highlighted by arrowheads) that are, according to Noirot and Quennedey (1974, 1991), characteristic of the cuticle overlying class 1 exocrine epidermal cells. These canals are similar to the pore canals that can be found in the common cuticle and that communicate with epicuticular filaments positioned immediately below the outer epicuticle but differ with respect to their width. As can be seen in the TEM images (Fig. 4b, c), the adhesion-mediating secretion crosses these canals as indicated by its presence within the small cavities traversing the electron-dense cuticle band. In the following reservoir (Fig. 10; As), the adhesion-mediating secretion can expand largely unhampered. Such large volume reservoirs are also found in other tarsal adhesive systems, e.g., within the euplantulae of *Tettigonia viridissima* (Orthoptera, Tettigoniidae) studied by Henning (1974), who describes this volume (termed "X-layer") as an exceptional layer of approximately 30 μm thickness including a liquid or viscous filling. The reservoir found in *G. portentosa* corresponds to this "X-layer" with regard to

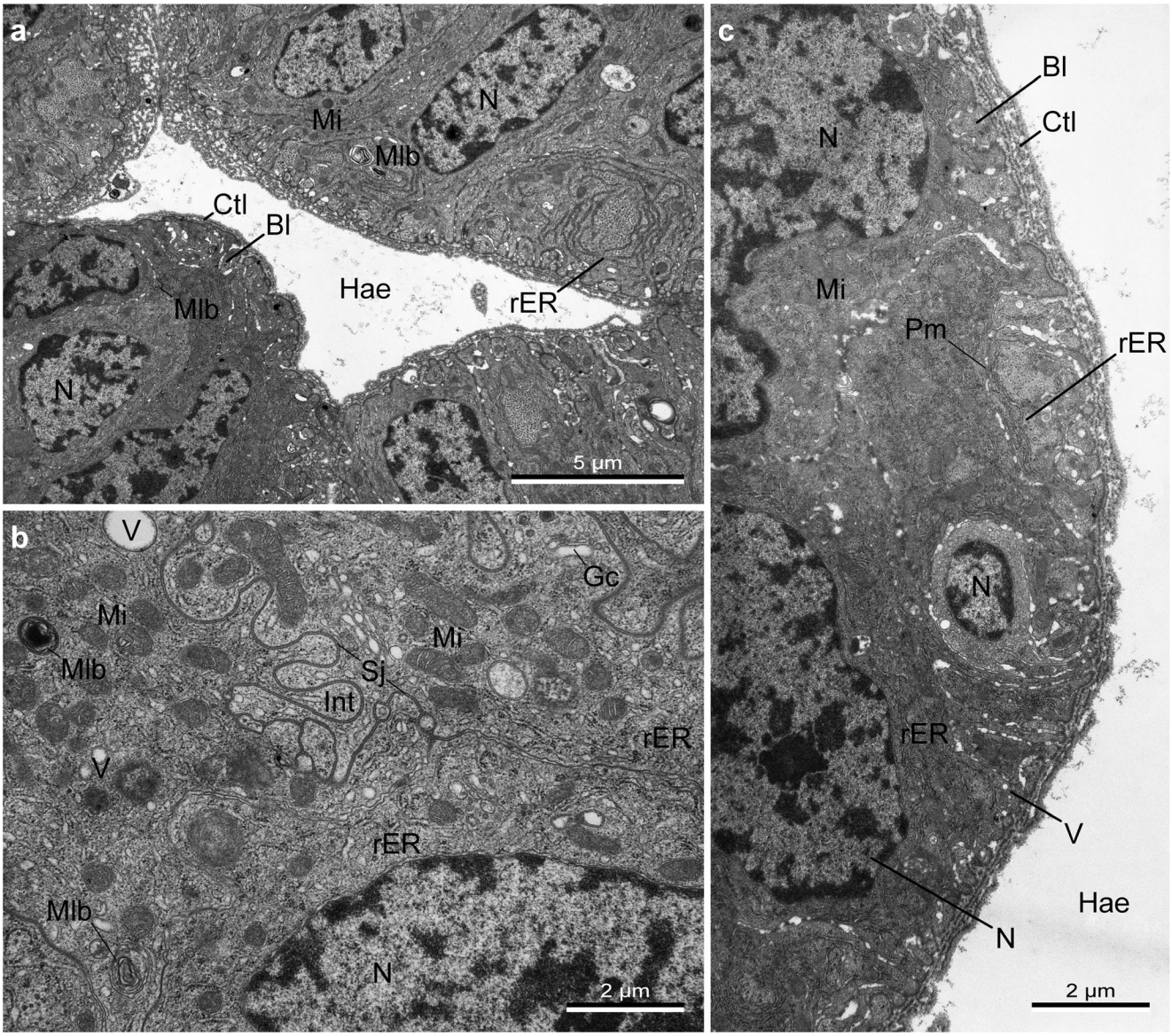

Fig. 8 Cross-sections through the arolium (protarsus) of *G. portentosa*. The detailed images relate to the central (**b**) and basal (**a**, **c**) area of the epidermal tissue. **a** The arrangement of basal poles of the epidermal cells surrounding a hemolymph reservoir. The nuclei are situated within the basal half of the cytoplasm. **c** Focus on the structure of the basal cell pole, which is characterized by a prominent basal labyrinth. **b** The high density of cellular components (especially mitochondria and rough-surfaced endoplasmic reticuli) around the nucleus and the interdigitations. *Bl* basal labyrinth; *Ctl* connective tissue-like layer; *Gc* Golgi complex; *Hae* hemolymph; *Int* interdigitations; *Mlb* multilamellar bodies; *Mi* mitochondria; *N* nucleus; *Pm* plasma membrane; *rER* rough-surfaced endoplasmic reticulum; *Sj* septate junction; *V* vesicle

both its position and dimension. In his listing of cuticle modifications being associated with class 1 exocrine cells, Quennedey (1998) also refers to the development of extracellular spaces allowing the storage of secretions. In his view, the simplest of those spaces arise from an enlargement of pore canals but can also develop between two cuticular layers, as found in our study. In such a case, this is often associated with a reduction of some middle cuticular layers. The distally adjacent layered cuticle (Fig. 10; Lc) that forms the interface between the inner and the outer endocuticle can be characterized by lamellae with microfibrils arranged in parallel (Fig. 4a, d), as has been shown for the tarsal cuticle in *Omocestus viridulus* (Orthoptera, Acrididae) (Schwarz and Gorb 2003). This layered cuticle area again contains a network of fine canals through which the adhesion-mediating secretion can diffuse to reach the sponge-like cuticle (Fig. 10; Slc). Within this layer, chitinous rods stretch to the interface of a ventral cuticle band bearing the fine epicuticle (cf., Figs. 4f, 10; vCb). Goodwyn et al. (2006) designate this electron-dense ventral cuticle band in the euplantulae of

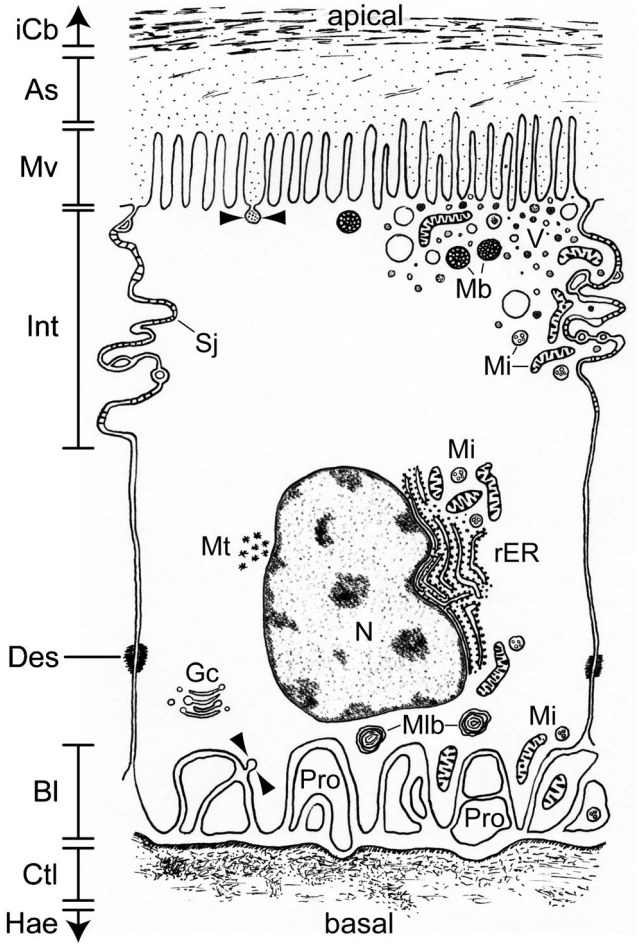

Fig. 9 Scheme of a representative exocrine epidermal cell of the arolium of *G. portentosa* giving an overview of the characteristic subcellular components. A detailed description of these structures is provided in the text. *As* adhesion-mediating secretion; *Bl* basal labyrinth; *Ctl* connective tissue-like layer; *Des* desmosome; *Gc* Golgi complex; *Hae* hemolymph; iCb inner cuticle band; *Int* interdigitations; *Mb* multivesicular bodies; *Mlb* multilamellar bodies; *Mi* mitochondria; *Mt* microtubules; *Mv* microvilli; *N* nucleus; *Pro* projections of adjacent cells; *rER* rough-surfaced endoplasmic reticulum; *Sj* septate junction; *V* vesicles; *arrowheads* at the apical cell membrane, exocytosis; *arrowheads* at the basal cell membrane, pinocytosis

Locusta migratoria (Orthoptera, Acrididae) as a superficial layer that is penetrated by pore canals. In our study, these canals end in the transition area to the epicuticle (Fig. 4f; arrows).

Considering all of these layers, the sponge-like cuticle is the last reservoir that is able to store the adhesion-mediating secretion. To make this possible, the chitinous rods branch into several smaller strands, which taper off, thus forming a fine network, in whose cavities the secretion is localized. Neither in the epicuticle of the arolia nor on the surface of the euplantulae have we detected any excretory pores or openings through which the adhesion-mediating secretion could reach the external surface of the adhesive organs. This is in agreement with studies in *Musca domestica* (Hasenfuss 1977), *Calliphora erythrocephala* (Diptera, Muscidae) (Bauchhenß and Renner 1977), or *Megoura viciae* (Hemiptera, Aphididae) (Lees and Hardie 1988), who have also been unable to reveal the mode of excretion of the adhesion-mediating secretion, since no secretory pores have been found. The final passage through the outer cuticular wall is assumed to proceed via a system of extremely fine pore canals and epicuticular filaments of a few nanometers in diameter (cf., Lees and Hardie 1988), as this is a general pathway of lipid secretion in the insect cuticle (reviewed in Betz 2010).

In conclusion, the cuticle associated with the adhesive organs of *G. portentosa* can be considered as an alternating sequence of layers having various properties with respect to their ability to store, distribute, and transmit the adhesion-mediating secretion. On the one hand, large storage cavities exist within which the secretion can freely move and be laterally distributed. On the other hand, denser cuticle bands are present through which the adhesion-mediating secretion must penetrate via fine pore canals with a lower transmission rate. In combination, this sequence of layers with different properties might result in an optimal hydrostatic counter pressure that arises as soon as the adhesive organ comes into contact with the surface structures of the substrate and thus optimize (maximize) its true contact area. This agrees with Bennemann et al. (2014), who have analyzed the Young's modulus of the cuticle of the arolia in the stick insect *Carausius morosus* (Phasmatodea, Phasmatidae) by means of indentation experiments. The authors have found that the hydroflation of the pretarsus and several layers of the cuticle (depending on the indentation depth) have an effect on the deformation behavior of the adhesive organ. Moreover, Federle et al. (2001), Jarau et al. (2005), and Billen (2009) have discussed the role of the secretion within the arolium of ants and bees with regard to a hydraulic function. In their study dealing with the production of tarsal adhesion-mediating secretion in *C. morosus* and *Nauphoeta cinerea* (Blattodea, Blaberidae), Dirks and Federle (2011) have analyzed the function of the cuticle of the adhesive organ with regard to the ability of the cuticle to store secretion fluids. They have therefore evaluated the volume of secretion (footprints) deposited on a substrate during consecutive press-downs and found that the volume decreases exponentially reaching a non-zero steady-state after some time (approx. 7–10 steps). After a short recovery period (approx. 15 min), the footprints regain their original volume indicative of the presence of a storage reservoir within the branched fibrous structures of the cuticle (Fig. 10) that is supplied with secretions at a steady rate. The authors assume that the adhesive fluid is transported into the contact zone with the substratum by compression of the pad or by capillary suction resulting from the contact with the surface, i.e., when the soft adhesive structures are deformed. In *G. portentosa*, multiple linearly arranged sub-reservoirs might help further to delay

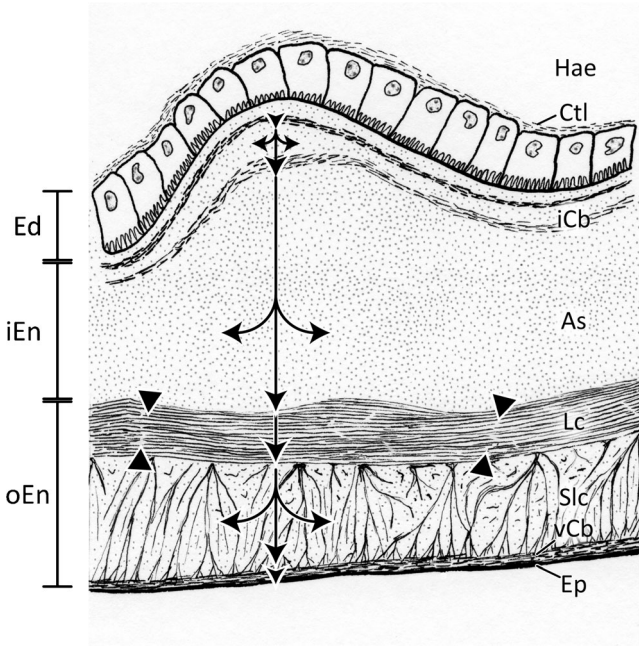

Fig. 10 Scheme of a cross-section through the euplantula of *G. portentosa*. The layered cuticle is associated with the exocrine epidermal tissue that excretes the adhesion-mediating secretion into a subcuticular reservoir. On its way to the exterior, the secretion fluid has to pass several cuticle layers and reservoir-like cavities. Whereas the secretion can be distributed freely across the large cavities (indicated by *arrows* pointing in various directions), this becomes increasingly difficult as the cuticle bands become denser and less permeable to the fluid. Within these layers, the secretion passes the cuticle through numerous small canals (indicated by *common arrows* or *arrow-heads*). The scheme also reflects the morphology of the cuticle of the arolia to a large extent. However, the cuticular layers of the arolia are subdivided by only one cuticle band and the sponge-like cuticle is thicker. *As* adhesion-mediating secretion; *Ctl* connective tissue-like layer; *Ed* epidermis; *Ep* epicuticle; *Hae* hemolymph; *iCb* pair of inner cuticle bands; *iEn* inner part of endocuticle; *Lc* layered cuticle; *oEn* outer part of endocuticle; *Slc* sponge-like cuticle; *vCb* ventral cuticle band; *arrows* indicate the direction of the adhesion-mediating secretion on its way through reservoir-like regions (different directions) or through small canals in denser cuticle regions (*common arrow*). *Black triangles* within the layered cuticle indicate pore canals

the fluid flow across the attachment organ from the epidermis toward the exterior. In their compartment model of fluid flow in insect tarsal attachment organs, Dirks and Federle (2011) postulate an "overflow" feedback mechanism that prevents the excessive production of adhesion-mediating secretion. To what extent the insertion of several smaller (instead of one large) sub-reservoirs prior to the sponge-like cuticle (as suggested by our findings) might improve such feedback mechanism and the overall control of the transport of the adhesive fluid toward the exterior remains to be investigated.

In addition, in view of the emulsion-like semi-solid nature of the adhesive (Gerhardt et al. 2015, 2016), the first two subcuticular spaces adjacent to the epidermal layer might separately take up its polar and non-polar fractions. Only after their release into these subspaces, might they be arranged into the final emulsion structure that soaks into the sponge-like cuticle by capillary action (Fig. 10; Slc).

Fourth level of hierarchy: Arolia and euplantulae as organs optimized for attachment and detachment during the locomotion process

During walking and climbing, two opposing crucial tasks have to be accomplished by the tarsal adhesive organs. First, they must generate sufficient adhesion and friction during attachment in order to interact safely with the substrate. However, at the same time, they should be detachable as rapidly and energy-efficiently as possible (e.g., Clemente and Federle 2008; Labonte and Federle 2013). With respect to the attachment process, the smooth tarsal adhesive pads are optimized to adapt to the asperities of substrates at various scales and thus to increase the real contact area and the contact perimeter. Consequently, they are able to achieve stronger adhesion and friction forces (cf., Gorb and Scherge 2000; Gorb et al. 2000; Jiao et al. 2000; Goodwyn et al. 2006). In accordance with Gorb et al. (2000) and Goodwyn et al. (2006), the compliant cushion-like appearance of the adhesive organs results largely from their inner morphology, i.e., the distribution and architecture of the chitinous rods interacting with the adhesion-mediating secretion and the epicuticle at the surface (cf., Figs. 2, 3). For orthopterans, two levels of deformation have been described in the euplantulae. The first level relates to the intimate contact formation with surface asperities of surface roughness attributable to the elastic deformation of secondary filaments located in the uppermost layer of the cuticle. This corresponds well with the layer of branched rods shown in Fig. 2c and characterized by the numerous fine fibers that branch outwards in a conical manner. The second level of deformation complies with the bending of the primary filaments corresponding to the principal fibers found in the arolium of *G. portentosa* (Fig. 2c; Lpr). This is also true for the euplantulae, but here, the sponge-like cuticle is thinner. Michels et al. (2016) analyzed the structure and properties of orthopteran adhesive pads (euplantulae) with a special focus on the distribution of the rubber-like protein resilin throughout the exocuticle. They were able to show the presence of a material gradient within the euplantulae: the layers of primary and branching rods inside the pad showed a high content of resilin constituting a "soft core", whereas the absence of resilin incorporation in the superficial layer results in the formation of stiff outer layer which keeps the position of the relatively long and thin fibers constant. Among other properties, such a stiffer outer layer might help to facilitate the re-release of the adhesive pads during regular locomotion (Michels et al. 2016; Betz et al. 2017). The adhesion-

mediating secretion within the sponge-like cuticle contributes to the visco-elastic behavior of the adhesive organs. This is because the adhesive fluid is displaced in regions to which an external force is applied and thus is distributed into other cavities within the sponge-like cuticle (Gorb et al. 2000; Goodwyn et al. 2006). According to Bennemann et al. (2014), the epicuticle might also play an important role in this context, since it can passively (by hydrostatic counter pressure) fold around asperities higher than its own thickness (i.e., "the thickness of the thin coverage is smaller than the wavelength of the roughness of the substrate"). This is relevant for systems in which the Young's modulus of the epicuticle exceeds that of the underlying endocuticle. In *G. portentosa*, the epicuticle of the arolia has a thickness of approx. 80 nm (euplantulae: approx. 30 nm), which might considerably affect the area of real contact, especially for substrates with small asperities, and thus also increase adhesion. Bennemann et al. (2014) analyzed this effect in the arolia of *C. morosus* and determined a thickness of its epicuticle of 225 nm.

Similarly to the attachment process, structures and behavioral patterns also affect fast and energy-efficient detachment. In a series of tribometrical performance experiments of both the euplantulae and the arolia of *G. portentosa*, Betz et al. (2017) have found various adaptations both on a morphological level and on the level of the adhesion-mediating secretion that might facilitate the detachment of these structures. Therefore, the adhesion (i.e., the force needed to detach the adhesive organ in a pull-off direction perpendicular to the substrate surface) and friction forces (i.e., the force needed to slide the adhesive pads parallel to the substrate surface) were determined in non-manipulated euplantulae and in euplantulae to which an artificial secretion fluid (squalan, squalan-based emulsion) was applied. The results of these studies indicate that, on smooth to nanorough surfaces during friction, the thin natural secretion film seems to adopt the function of a lubricant preventing immoderate friction forces. On rougher surfaces, other functions of the secretion, such as the amplification of the true contact surface by keeping the cuticle compliable, seem to pre-dominate. In addition, the adhesion measurements of Betz et al. (2017) suggest a viscous dissipation reducing effect of the semi-solid (grease-like) adhesion-mediating secretion; this is functionally supported by certain structural properties of the cuticle itself. As shown in Figs. 2, 4 and 10 and as described above, the sponge-like cuticle of the adhesion organs consists of chitinous rods that run almost perpendicularly to the uppermost layer bearing the epicuticle. During the detachment of the adhesive organs, these structures may enhance the tensile strength in a vertical direction thereby leading, together with the semi-solid consistency of the adhesion-mediating secretion, to a premature tear-off of the adhesive thread and thus to a moderate force being required to detach these structures (see Fig. 6b in Betz et al. 2017).

Conclusion

The Madagascar hissing cockroach *G. portentosa* is a skillful climber, even on smooth surfaces; however, it predominantly lives in litter (van Casteren and Codd 2010). The present study focuses on the ultramorphology of the arolium and the euplantulae of this insect as these mediate adhesive and frictional forces to the substratum. Whereas previous studies on *G. portentosa* have investigated the attachment performance of these organs and the chemical composition of the adhesion-mediating secretion released from their surface, the present work contributes to our understanding of their ultramorphology and considers both the structure of the glandular epithelium and the associated cuticle. The study reveals considerable differences from the general structure and organization of cuticle, differences that can be explained by the specific functions required in the production, storage, and release of an adhesive fluid, and at the same time, the establishment of a compliable interface to the outer environment. The application of both (Cryo-)SEM and TEM has made it possible to interweave structural aspects that apply to the cellular production of the adhesion-mediating secretion and those that apply to the storage and release of this secretion via various cuticle layers each showing their own peculiarities. The resulting interior compartmentalization of the attachment pads might contribute to both the final constitution of the emulsion structure of the adhesive and its controlled final release. On the other hand, studies on the viscoelastic properties of the cuticle of the smooth attachment pads also emphasize the functional significance of the internal layers with respect to its overall deformation behavior during locomotion on surfaces of diverse topographies (e.g., Gorb et al. 2000; Scholz et al. 2008; Bennemann et al. 2014). Further detailed studies will be necessary to disentangle all these functional aspects and to relate them to the overall ultramorphology of the adhesive pads as presented in this contribution.

Acknowledgements We thank Monika Meinert for technical assistance with the Cryo-SEM and Anja Schmitt for proof reading. Theresa Jones corrected the English.

Compliance with ethical standards

Funding This study was funded by a grant from the German Science Foundation DFG (grant number PAK 478) to Oliver Betz.

Conflict of interest The authors declare that they have no conflict of interest.

References

Alsop DW (1978) Comparative analysis of the intrinsic leg musculature of the American cockroach, *Periplaneta americana* (L.) J Morphol 158:199–241

Arnold JW (1974) Adaptive features on the tarsi of cockroaches (Insecta: Dictyoptera). Int J Insect Morphol Embryol 3:317–334

Bauchhenß E (1979) Die Pulvillen von *Calliphora erythrocephala* (Diptera, Brachycera) als Adhäsionsorgane. Zoomorphologie 93: 99–123

Bauchhenß E, Renner M (1977) Pulvillus of *Calliphora erythrocephala* Meig. (Diptera: Calliphoridae). Int J Insect Morphol Embryol 6: 225–227

Bennemann M, Backhaus S, Scholz I, Park D, Mayer J, Baumgartner W (2014) Determination of the Young's modulus of the epicuticle of the smooth adhesive organs of *Carausius morosus* using tensile testing. J Exp Biol 217:3677–3687

Bergmann P, Laumann M, Heethoff M (2010) Ultrastructural aspects of vitellogenesis in *Archegozetes longisetosus* Aoki, 1965 (Acari, Oribatida, Trhypochthoniidae). Soil Org 82:193–208

Bergmann P, Heethoff M (2012) Development of the internal reproductive organs in early nymphal stages of *Archegozetes longisetosus* Aoki (Acari, Oribatida, Trhypochthoniidae) as obtained by synchrotron X-ray microtomography (SR-μCT) and transmission electron microscopy (TEM). Soil Org 84:459–470

Betz O (2002) Performance and adaptive value of tarsal morphology in rove beetles of the genus *Stenus* (Coleoptera, Staphylinidae). J Exp Biol 205:1097–1113

Betz O (2003) Structure of the tarsi in some *Stenus* species (Coleoptera, Staphylinidae): external morphology, ultrastructure, and tarsal secretion. J Morphol 255:24–43

Betz O (2010) Adhesive exocrine glands in insects: morphology, ultrastructure, and adhesive secretion. In: Byern J, Grunwald I (eds) Biological adhesive systems. From nature to technical and medical application. Springer, Berlin, pp 111–152

Betz O, Mumm R (2001) The predatory legs of *Philonthus marginatus* (Coleoptera, Staphylinidae): functional morphology and tarsal ultrastructure. Arthropod Struct Dev 30:77–97

Betz O, Maurer A, Verheyden AN, Schmitt C, Kowalik T, Braun J, Grunwald I, Hartwig A, Neuenfeldt M (2016) First protein and peptide characterization of the tarsal adhesive secretions in the desert locust, *Schistocerca gregaria*, and the Madagascar hissing cockroach, *Gromphadorhina portentosa*. Insect Mol Biol 25:541–549

Betz O, Frenzel M, Steiner M, Vogt M, Kleemeier M, Hartwig A, Sampalla B, Rupp F, Boley M, Schmitt C (2017) Adhesion and friction of the smooth attachment system of the cockroach *Gromphadorhina portentosa* and the influence of the application of fluid adhesives. Biol Open 6:589–601

Beutel RG, Gorb SN (2001) Ultrastructure of attachment specializations of hexapods (Arthropoda): evolutionary patterns inferred from a revised ordinal phylogeny. J Zool Syst Evol Res 39:177–207

Billen J (2009) Occurrence and structural organization of the exocrine glands in the legs of ants. Arthropod Struct Dev 38:2–15

Bullock JMR, Drechsler P, Federle W (2008) Comparison of smooth and hairy attachment pads in insects: friction, adhesion and mechanisms for direction-dependence. J Exp Biol 211:3333–3343

Bullock JMR, Federle W (2009) Division of labour and sex differences between fibrillar, tarsal adhesive pads in beetles: effective elastic modulus and attachment performance. J Exp Biol 212:1876–1888

Cassier P, Lensky Y (1995) Ultrastructure of the wax gland complex and secretion of beeswax in the worker honey bee *Apis mellifera* L. Apidologie 26:17–17

Claude P, Goodenough DA (1973) Fracture faces of zonulae occludentes from "tight" and "leaky" epithelia. J Cell Biol 58:390–400

Clemente CJ, Federle W (2008) Pushing versus pulling: division of labour between tarsal attachment pads in cockroaches. Proc R Soc Lond B 275:1329–1336

Costa-Leonardo AM (2001) The frontal weapon of the termite *Armitermes euamignathus* Silvestri (Isoptera, Termitidae, Nasutitermitinae). Rev Bras Zool 18:411–419

Del Cerro M, Cogen J, Del Cerro C (1980) Stevenel's blue, an excellent stain for optical microscopical study of plastic embedded tissues. Microsc Acta 83:117–121

Dewitz H (1884) Ueber die Fortbewegung der Thiere an senkrechten glatten Flächen vermittelst eines Secretes. Pflügers Arch Ges Physiol Mensch Tiere 33:440–481

Dirks JH (2014) Physical principles of fluid-mediated insect attachment-Shouldn't insects slip? Beilstein J Nanotechnol 5:1160–1166

Dirks JH, Clemente CJ, Federle W (2010) Insect tricks: two-phasic foot pad secretion prevents slipping. J R Soc Interface 7:587–593

Dirks JH, Federle W (2011) Mechanisms of fluid production in smooth adhesive pads of insects. J R Soc Interface 8:952–960

Dixon AFG, Croghan PC, Gowing RP (1990) The mechanism by which aphids adhere to smooth surfaces. J Exp Biol 152:243–253

Drechsler P, Federle W (2006) Biomechanics of smooth adhesive pads in insects: influence of tarsal secretion on attachment performance. J Comp Physiol A 192:1213–1222

Eberhard MJ, Pass G, Picker MD, Beutel R, Predel R, Gorb SN (2009) Structure and function of the arolium of Mantophasmatodea (Insecta). J Morphol 270:1247–1261

Eisner T, Aneshansley DJ (2000) Defense by foot adhesion in a beetle (*Hemisphaerota cyanea*). Proc Natl Acad Sci U S A 97:6568–6573

Fawcett DW (1981) The cell. W. B. Saunders, Philadelphia

Federle W, Brainerd EL, McMahon TA, Hölldobler B (2001) Biomechanics of the movable pretarsal adhesive organ in ants and bees. Proc Natl Acad Sci U S A 98:6215–6220

Federle W, Riehle M, Curtis ASG, Full RJ (2002) An integrative study of insect adhesion: mechanics and wet adhesion of pretarsal pads in ants. Integr Comp Biol 42:1100–1106

Federle W, Endlein T (2004) Locomotion and adhesion: dynamic control of adhesive surface contact in ants. Arthropod Struct Dev 33:67–75

Frantevich L, Gorb SN (2004) Structure and mechanics of the tarsal chain in the hornet, *Vespa crabro* (Hymenoptera: Vespidae): implications on the attachment mechanism. Arthropod Struct Dev 33:77–89

Geiselhardt SF, Geiselhardt S, Peschke K (2009) Comparison of tarsal and cuticular chemistry in the leaf beetle *Gastrophysa viridula* (Coleoptera: Chrysomelidae) and an evaluation of solid-phase microextraction and solvent extraction techniques. Chemoecology 19:185–193

Geiselhardt SF, Lamm S, Gack C, Peschke K (2010) Interaction of liquid epicuticular hydrocarbons and tarsal adhesive secretion *in Leptinotarsa decemlineata* Say (Coleoptera: Chrysomelidae). J Comp Physiol A 196:369–378

Gerhardt H, Schmitt C, Betz O, Albert K, Lämmerhofer M (2015) Contact solid-phase microextraction with uncoated glass and polydimethylsiloxane-coated fibers versus solvent sampling for the determination of hydrocarbons in adhesion secretions of Madagascar hissing cockroaches *Gromphadorrhina portentosa* (Blattodea) by gas chromatography-mass spectrometry. J Chromatogr A 1388:24–35

Gerhardt H, Betz O, Albert K, Lämmerhofer M (2016) Insect adhesion secretions: similarities and dissimilarities in hydrocarbon profiles of tarsi and corresponding tibiae. J Chem Ecol 42:725–738

Goodwyn PP, Peressadko A, Schwarz H, Kastner V, Gorb SN (2006) Material structure, stiffness, and adhesion: why attachment pads of the grasshopper (*Tettigonia viridissima*) adhere more strongly than those of the locust (*Locusta migratoria*) (Insecta: Orthoptera). J Comp Physiol A 192:1233–1243

Gorb SN (1998) The design of the fly adhesive pad: distal tenent setae are adapted to the delivery of an adhesive secretion. Proc R Soc Lond B 265:747–752

Gorb SN (2007) Smooth attachment devices in insects: functional morphology and biomechanics. Adv Insect Phys 34:81–115

Gorb SN, Gorb E, Kastner V (2001) Scale effects on the attachment pads and friction forces in syrphid flies (Diptera, Syrphidae). J Exp Biol 204:1421–1431

Gorb SN, Jiao Y, Scherge M (2000) Ultrastructural architecture and mechanical properties of attachment pads in *Tettigonia viridissima* (Orthoptera Tettigoniidae). J Comp Physiol A 186:821–831

Gorb SN, Scherge M (2000) Biological microtribology: anisotropy in frictional forces of orthopteran attachment pads reflects the ultrastructure of a highly deformable material. Proc R Soc Lond B 267: 1239–1244

Hasenfuss I (1977) Die Herkunft der Adhäsionsflüssigkeit bei Insekten. Zoomorphologie 87:51–64

Henning B (1974) Morphologie und Histologie der Tarsen von *Tettigonia viridissima* L. (Orthoptera, Ensifera). Z Morphol Tiere 79:323–342

Hepburn HR, Bernard RTF, Davidson BC, Muller WJ, Lloyd P, Kurstjens SP, Vincent SL (1991) Synthesis and secretion of beeswax in honeybees. Apidologie 22:21–36

Ishii S (1987) Adhesion of a leaf feeding ladybird *Epilachna vigintioctomaculta* (Coleoptera: Coccinellidae) on a vertically smooth surface. Appl Entomol Zool 22:222–228

Jarau S, Hrncir M, Zucchi R, Barth FG (2005) Morphology and structure of the tarsal glands of the stingless bee *Melipona seminigra*. Naturwissenschaften 92:147–150

Jiao Y, Gorb SN, Scherge M (2000) Adhesion measured on the attachment pads of *Tettigonia viridissima* (Ortoptera, Insecta). J Exp Biol 203:1887–1895

Kendall MD (1970) The anatomy of the tarsi of *Schistocerca gregaria* Forskål. Z Zellforsch Mikrosk Anat 109:112–137

Kosaki A, Yamaoka R (1996) Chemical composition of footprints and cuticula lipids of three species of lady beetles. Jpn J Appl Entomol Zool 40:47–53

Labonte D, Federle W (2013) Functionally different pads on the same foot allow control of attachment: stick insects have load-sensitive "heel" pads for friction and shear-sensitive "toe" pads for adhesion. PLoS ONE 8:e81943

Lane NJ, Skaer HL, Swales LS (1977) Intercellular junctions in the central nervous system of insects. J Cell Sci 26:175–199

Langer MG, Ruppersberg JP, Gorb SN (2004) Adhesion forces measured at the level of a terminal plate of the fly's seta. Proc R Soc Lond B 271:2209–2215

Laumann M, Bergmann P, Norton RA, Heethoff M (2010) First cleavages, preblastula and blastula in the parthenogenetic mite *Archegozetes longisetosus* (Acari, Oribatida) indicate holoblastic rather than superficial cleavage. Arthropod Struct Dev 39:276–286

Lees AD, Hardie JIM (1988) The organs of adhesion in the aphid *Megoura viciae*. J Exp Biol 136:209–228

Michels J, Appel E, Gorb SN (2016) Functional diversity of resilin in Arthropoda. Beilstein J Nanotech 7:1241–1259

Müller CH, Rosenberg J, Hilken G (2014) Ultrastructure, functional morphology and evolution of recto-canal epidermal glands in Myriapoda. Arthropod Struct Dev 43:43–61

Niederegger S, Gorb SN, Jiao Y (2002) Contact behaviour of tenent setae in attachment pads of the blowfly *Calliphora vicina* (Diptera, Calliphoridae). J Comp Physiol A 187:961–970

Noirot CH, Quennedey A (1974) Fine structure of insect epidermal glands. Annu Rev Entomol 19:61–80

Noirot CH, Quennedey A (1991) Glands, gland cells, glandular units: some comments on terminology and classification. Ann Soc Entomol Fr 2:123–128

Piechocki R, Händel J (2007) Makroskopische Präparationstechnik: Wirbellose. Leitfaden für das Sammeln, Präparieren und Konservieren, 5th edn. Schweizerbart'sche, Stuttgart

Quennedey A (1975) Morphology of exocrine glands producing pheromones and defensive substances in subsocial and social insects. Proceedings of the IUSSI Symposium, Dijon, pp 1–21

Quennedey A (1998) Insect epidermal gland cells: ultrastructure and morphogenesis. In: Harrison FW, Locke M (eds) Microscopic anatomy of invertebrates, vol 11A. Insecta, Wiley, New York, pp 177–207

Reiz M, Gerhardt H, Schmitt C, Betz O, Albert K, Lämmerhofer M (2015) Analysis of chemical profiles of insect adhesion secretions by gas chromatography-mass spectrometry. Anal Chim Acta 854: 47–60

Roth LM, Willis ER (1952) Tarsal structure and climbing ability of cockroaches. J Exp Biol 119:483–517

Scholz I, Baumgartner W, Federle W (2008) Micromechanics of smooth adhesive organs in stick insects: pads are mechanically anisotropic and softer towards the adhesive surface. J Comp Physiol A 194: 373–384

Schwarz H, Gorb SN (2003) Method of platinum-carbon coating of ultrathin sections for transmission and scanning electron microscopy: an application for study of biological composites. Microsc Res Tech 62:218–224

Serrão JE, Castrillon MI, dos Santos-Mallet JR, Zanuncio JC, Gonçalves TCM (2008) Ultrastructure of the salivary glands in *Cimex hemipterus* (Hemiptera: Cimicidae). J Med Entomol 45:991–999

Stork NE (1980) A scanning electron microscope study of tarsal adhesive setae in the Coleoptera. Zool J Linn Soc 68:173–306

van Casteren A, Codd JR (2010) Foot morphology and substrate adhesion in the Madagascan hissing cockroach, *Gromphadorhina portentosa*. J Insect Sci 10:40

Vincent JF, Wegst UG (2004) Design and mechanical properties of insect cuticle. Arthropod Struct Dev 33:187–199

Vötsch W, Nicholson G, Müller R, Stierhof Y-D, Gorb SN, Schwarz U (2002) Chemical composition of the attachment pad secretion of the locust *Locusta migratoria*. Insect Biochem Mol Biol 32:1605–1613

Voigt D, Schuppert JM, Dattinger S, Gorb SN (2008) Sexual dimorphism in the attachment ability of the Colorado potato beetle *Leptinotarsa decemlineata* (Coleoptera: Chrysomelidae) to rough substrates. J Insect Physiol 54:765–776

Walker G, Yulf AB, Ratcliffe J (1985) The adhesive organ of the blowfly, *Calliphora vomitoria*: a functional approach (Diptera: Calliphoridae). J Zool 205:297–307

Weirauch C (2007) Hairy attachment structures in Reduviidae (Cimicomorpha, Heteroptera), with observations on the fossula spongiosa in some other Cimicomorpha. Zool Anz 246:155–175

Zhou Y, Robinson A, Viney C, Federle W (2015) Effect of shear forces and ageing on the compliance of adhesive pads in adult cockroaches. J Exp Biol 218:2775–2781

Zill SN, Keller BR, Chaudhry S, Duke ER, Neff D, Quinn R, Flannigan C (2010) Detecting substrate engagement: responses of tarsal campaniform sensilla in cockroaches. J Comp Physiol A 196:407–420